INTERNATIONAL JOURNAL FOR NUMERICAL METHODS IN FLUIDS
Int. J. Numer. Meth. Fluids 2010; **62**:24–55
Published online 26 February 2009 in Wiley InterScience (www.interscience.wiley.com). DOI: 10.1002/fld.2011

Nonreflecting boundary conditions based on nonlinear multidimensional characteristics

Qianlong Liu[1] and Oleg V. Vasilyev[2,*,†]

[1]*Department of Mechanical Engineering, The Johns Hopkins University, Baltimore, MD 21218, U.S.A.*
[2]*Department of Mechanical Engineering, University of Colorado, 427 UCB, Boulder, CO 80309, U.S.A.*

SUMMARY

Nonlinear characteristic boundary conditions based on nonlinear multidimensional characteristics are proposed for 2- and 3-D compressible Navier–Stokes equations with/without scalar transport equations. This approach is consistent with the flow physics and transport properties. Based on the theory of characteristics, which is a rigorous mathematical technique, multidimensional flows can be decomposed into acoustic, entropy, and vorticity waves. Nonreflecting boundary conditions are derived by setting corresponding characteristic variables of incoming waves to zero and by partially damping the source terms of the incoming acoustic waves. In order to obtain the resulting optimal damping coefficient, analysis is performed for problems of pure acoustic plane wave propagation and arbitrary flows. The proposed boundary conditions are tested on two benchmark problems: cylindrical acoustic wave propagation and the wake flow behind a cylinder with strong periodic vortex convected out of the computational domain. This new approach substantially minimizes the spurious wave reflections of pressure, density, temperature, and velocity as well as vorticity from the artificial boundaries, where strong multidimensional flow effects exist. The numerical simulations yield accurate results, confirm the optimal damping coefficient obtained from analysis, and verify that the method substantially improves the 1-D characteristics-based nonreflecting boundary conditions for complex multidimensional flows. Copyright © 2009 John Wiley & Sons, Ltd.

Received 4 September 2008; Revised 19 December 2008; Accepted 7 January 2009

KEY WORDS: nonreflecting boundary conditions; nonlinear multidimensional characteristics; complex multidimensional flows; compressible Navier–Stokes equations; LODI; spurious wave reflection

*Correspondence to: Oleg V. Vasilyev, Department of Mechanical Engineering, University of Colorado, 427 UCB, Boulder, CO 80309, U.S.A.
†E-mail: oleg.vasilyev@colorado.edu

Contract/grant sponsor: National Aeronautics and Space Administration; contract/grant number: NAG-1-02116
Contract/grant sponsor: National Science Foundation; contract/grant numbers: EAR-0242591, EAR-0327269, ACI-0242457

1. INTRODUCTION

For computational efficiency and affordability purposes, the use of a sufficiently small computational domain is often required for flow simulations of physical and engineering interest. This necessitates the introduction of artificial computational boundaries. In order to obtain an accurate time-dependent numerical simulation of the flow, spurious nonphysical wave reflections from the artificial boundary need to be minimized. Several techniques for the creation of artificial computational boundaries have been developed, namely linearized boundary conditions, absorbing layers, and nonlinear characteristic boundary conditions. The readers are referred to informative reviews [1–4] on the subject. In this paper, nonreflecting boundary conditions for nonlinear multidimensional general flows are developed based on a rigorous mathematical technique. The proposed boundary conditions are consistent to the flow physics and thus minimize the spurious wave reflections from the artificial boundaries.

The theoretical basis for nonreflecting boundary conditions was set by Engquist and Majda [5, 6]. They developed a systematic pseudo-differential operator technique to exactly annihilate outgoing waves so as to construct a hierarchy of local nonreflecting boundary conditions for linear systems. All these local approximations for exact boundary conditions using the polynomial or rational function approximation, together with other boundary conditions [7, 8], give very accurate solutions for linearized multidimensional flows, e.g. the classical wave equation. However, there is apparently no extension for the nonlinear multidimensional flows and, thus, they are not suitable for the nonlinear multidimensional flows. For the absorbing layer approach, including the techniques of a perfectly matched layer [9, 10], Freund's buffer zone [11], and fringe methods [12], modified governing equations are considered in the adjacent regions of the artificial boundaries, which adds additional computational costs. Although some of them give good results for specific problems, they generally have many free parameters, which need to be carefully tuned for new problems in order to obtain satisfactory solutions. Furthermore, their extension for nonlinear multidimensional flows are not straightforward and need further investigation. On the other hand, Poinsot and Lele's nonlinear 1-D characteristic boundary conditions [13] remain widely used in compressible flow simulations due to simplicity and robustness and have been proven very useful, although they generate strong spurious reflections for realistic nonlinear multidimensional flows.

The main idea of Engquist and Majda's nonreflecting boundary condition is 'the characteristic variables corresponding to incoming characteristic curves are constant' for linearized systems [14]. Hedstrom [14] extended it to the 1-D nonlinear system based on 1-D nonlinear characteristics. This 1-D approximation of characteristic boundary conditions was further extended to multidimensional Euler equations by Thompson [15, 16]. Poinsot and Lele [13] extended Thompson's approach to the multidimensional Navier–Stokes equations and obtain the well-known Navier–Stokes characteristic boundary conditions (NSCBC). This approach makes the locally 1-D inviscid (LODI) assumption such that the waves are normal to the artificial computational boundary. The NSCBC has been extended to multicomponent perfect gas reactive flows by Baum *et al.* [17] and Moureau *et al.* [18], multicomponent real gas mixture by Okong'o and Bellan [19], and generalized coordinates by Kim and Lee [20, 21]. For the 1-D flows, NSCBC gives the exact boundary conditions. However, for the nonlinear multidimensional flows, it generates strong spurious wave reflections of pressure, density, velocity, and temperature from the artificial boundaries, especially for the outflow boundary, where complex flow structures exist and the nonlinear multidimensional effects are strong. These spurious wave reflections result from three shortcomings of the LODI approach for the actual nonlinear multidimensional flows: the use of 1-D characteristics, the consideration of characteristics only

DOI: 10.1002/fld

in the direction normal to the boundary, and the treatment of the transverse derivatives as source terms without any modification.

Various techniques, mostly in the context of 1-D characteristics, have been proposed to remedy the above-mentioned shortcomings for multidimensional flows. Nicoud [22] discussed the importance of the transverse terms for several approaches. Sutherland and Kennedy [23] recognized the inclusion of the chemical source terms in the LODI approach for reacting flows. This treatment allows flame propagation through the boundary without drastically affecting the solution on the interior. Prosser [24, 25] improved LODI approach for low Mach number flows using asymptotic analysis. Yoo *et al.* [26] and Yoo and Im [27] improved the LODI approach by incorporating the transverse terms to the characteristic wave amplitudes and by accommodating a relaxation treatment for the transverse gradient terms. It should be stressed that this approach works only for low Mach number flows and is invalid for general flows. First, the relaxation treatment is analogous to the approach of Rudy and Strikwerda [28], which was used to maintain pressure around a prescribed ambient value. This analogy does not hold for general flows, since the so-called desired steady value of incoming wave amplitude does not exist any more. Second, the corresponding relaxation coefficient was determined by the low Mach number asymptotic analysis. However, as indicated by the authors themselves, the approach of Yoo and Im [27] is far from ideal for high Mach number flow cases limit due to the inherent low Mach number assumptions. Lastly, there is no rigorous mathematical and/or physical reasoning in their definition of characteristic wave amplitudes by incorporating the transverse terms into 1-D characteristic wave amplitudes. This definition is mainly from the analogy and numerical tests for low Mach number flows. Liu [29] implemented the LODI approach in the oblique direction successfully for acoustic problems by implicitly calculating the local acoustic wave propagation direction. However, its straightforward extension for general flows does not seem to exist.

It is needed to point out that all of the above-mentioned improved methods possess the inherent limitations of 1-D nonlinear characteristics for multidimensional general flow simulations. In order to develop a consistent approach for nonlinear multidimensional general flows, it is natural to explore nonreflecting boundary conditions based on nonlinear multidimensional characteristics. For the details of the nonlinear multidimensional characteristics, we refer the reader to the classical computational gasdynamics textbook of Laney [30] and the note by Deconinck [31].

To minimize the spurious reflections for the nonlinear multidimensional flows, the nonlinear 1-D characteristic boundary conditions are extended to those based on nonlinear multidimensional characteristics. It should be stressed that the previous studies work only in low Mach number limit, while our approach is valid for general flows. In contrast to the methods mentioned above, our approach is based on the rigorous mathematical analysis for general flows, which is consistent with the flow physics. The definition of the characteristic wave amplitudes comes from the rigorous multidimensional characteristic analysis. Note that the present approach and the method discussed in References [26, 27] coincide with the low Mach number limit.

The 1-D characteristic analysis is straightforward while the multidimensional characteristic analysis is complicated but physical. The complexity and numerous free parameters arise for the multidimensional characteristic analysis. It is well known that the waves behave much differently in multi-dimensions than they do in one dimension. In 1-D flows, waves can propagate in two directions, left or right, and thus it is easy to identify the incoming waves. In contrast, waves may travel in infinite number of directions for multidimensional flows. A simple wave separation can be done easily for 1-D flows, which becomes impossible for multidimensional flows, since two Jacobian matrices do not commute and thus are not simultaneously diagonalizable. Characteristic

DOI: 10.1002/fld

variables are constant along characteristics for 1-D flows, which may not be true for multidimensional flows due to source terms. Although the complexity arises for the multidimensional wave analysis, multidimensional characteristics are consistent with the physics of flows and transport properties, when the flows are strongly multidimensional. In this paper, the 1-D characteristics approach is extended to the nonlinear multidimensional characteristic method. This new approach will be tested for two cases: oblique acoustic propagation and nonlinear wake flows. For the former case, which is a linear flow, Engquist and Majda's approach [5, 6] generates very accurate results. However, since the study of this paper is for nonlinear multidimensional general flows, this case, together with the latter case, is used to verify that the new approach significantly improves the nonlinear 1-D characteristic approach for multidimensional compressible general flows.

The rest of the paper is organized as follows. In Section 2, the multidimensional characteristic analysis is presented, 2-D characteristic boundary conditions are proposed, and optimal damping coefficients are derived for acoustic waves and general flows using mathematical analysis and physical argument. Numerical simulations of two benchmark problems on the cylindrical acoustic wave propagation and the flow around a cylinder generating strong periodic vortices in the wake region with complex flow structures are discussed in Section 3. Appendices provide other characteristic boundary conditions for 2- and 3-D flows, reactive flows, and the transport properties.

2. NONREFLECTING BOUNDARY CONDITIONS BASED ON MULTIDIMENSIONAL CHARACTERISTICS

2.1. Governing equations

The governing nondimensional Navier–Stokes equations for viscous compressible flows are

$$\frac{\partial \rho}{\partial t} = -\frac{\partial m_j}{\partial x_j} \tag{1}$$

$$\frac{\partial m_i}{\partial t} = -\frac{\partial}{\partial x_j}(m_i u_j) - \frac{\partial p}{\partial x_i} + \frac{1}{Re_a}\frac{\partial \tau_{ij}}{\partial x_j} \tag{2}$$

$$\frac{\partial e}{\partial t} = -\frac{\partial}{\partial x_j}[(e+p)u_j] + \frac{1}{Re_a}\frac{\partial}{\partial x_j}(u_i \tau_{ij}) + \frac{1/(\gamma-1)}{Re_a Pr}\frac{\partial}{\partial x_j}\left(\mu \frac{\partial T}{\partial x_j}\right) \tag{3}$$

where

$$p = \rho T/\gamma, \quad \tau_{ij} = \mu\left(\frac{\partial u_i}{\partial x_j} + \frac{\partial u_j}{\partial x_i} - \frac{2}{3}\frac{\partial u_k}{\partial x_k}\delta_{ij}\right), \quad e = \frac{1}{2}\rho u_i u_i + \frac{p}{\gamma-1}$$

ρ is the density of the fluid, $\mathbf{u} = (u_1, u_2, u_3)$ is the velocity, $m_j = \rho u_j$ is the mass flux, p is the pressure, τ_{ij} is the shear stress tensor, μ is the coefficient of temperature-dependent dynamic viscosity of the fluid, e is the total energy, T is the absolute temperature, and $\gamma = c_p/c_v$, $Re_a = \rho_0 c_0 L/\mu_0$ is the acoustic Reynolds number, and $Pr = \mu c_p/k$ is the Prandtl number. The variables of velocity, length, time, energy, density, pressure, viscosity, thermal conductivity, and temperature are, respectively, nondimensionalized by the reference speed of sound c_0, characteristic length L, L/c_0, c_0^2, the reference density ρ_0, $\rho_0 c_0^2$, the reference viscosity μ_0, $\mu_0 c_{p_0}$, and the reference temperature T_0.

DOI: 10.1002/fld

For efficiency and accuracy purposes, appropriate nonreflecting boundary conditions are required in addition to the governing equations for a relatively small computational domain.

2.2. Nonlinear multidimensional characteristics

Let us start the discussion of nonlinear multidimensional characteristics for 2-D flow simulations in a relatively small computational domain $\Omega=[x_1^{\min}, x_1^{\max}]\times[x_2^{\min}, x_2^{\max}]$. The 2-D Euler equations for primitive variables can be written in the vector form as follows:

$$\frac{\partial \mathbf{w}}{\partial t}+\mathbf{A}\frac{\partial \mathbf{w}}{\partial x_1}+\mathbf{B}\frac{\partial \mathbf{w}}{\partial x_2}=0 \tag{4}$$

where $\mathbf{w}=(\rho\ u_1\ u_2\ p)^{\mathrm{T}}$ is the vector of the primitive variables and the Jacobian matrices $\mathbf{A}$ and $\mathbf{B}$ are:

$$\mathbf{A}=\begin{bmatrix} u_1 & \rho & 0 & 0 \\ 0 & u_1 & 0 & \dfrac{1}{\rho} \\ 0 & 0 & u_1 & 0 \\ 0 & \rho c^2 & 0 & u_1 \end{bmatrix}, \quad \mathbf{B}=\begin{bmatrix} u_2 & 0 & \rho & 0 \\ 0 & u_2 & 0 & 0 \\ 0 & 0 & u_2 & \dfrac{1}{\rho} \\ 0 & 0 & \rho c^2 & u_2 \end{bmatrix}$$

where $c=T^{1/2}$ is the normalized local speed of sound. The nonlinear Euler equations can be rewritten in the most general [30] or limited [32, 33] characteristic forms by using the theory of characteristics. Note that all of the characteristic forms are mathematically equivalent to the vector form of Euler equations. These characteristic forms represent the physical interpretation of the mathematical equations for the nonlinear multidimensional flows. In this paper, one of the simplest nonlinear multidimensional characteristic forms is considered for simplicity purpose.

Based on the theory of characteristic, the physically relevant simple waves and their orientation can be determined [32, 33]. This leads to a straightforward and algebraically simple multidimensional characteristic decomposition of four waves: two acoustic waves, one vorticity wave, and one entropy wave. 1-D wave modelling of classical nonreflecting boundary conditions is inconsistent with flow physics. In contrast, this multidimensional wave analysis is consistent with the physics of flows and transport properties, and thus describes the multidimensional flows physically. The multidimensional characteristic form of Euler equations for an arbitrary unit vector $\hat{\mathbf{n}}=(n_{x_1}, n_{x_2})$, can be written as [30, 32, 33]:

$$\frac{\partial v_1}{\partial t}+\boldsymbol{\lambda}_1\cdot\nabla v_1=-c(n_{x_2}, -n_{x_1})\cdot\nabla v_3 \tag{5}$$

$$\frac{\partial v_2}{\partial t}+\boldsymbol{\lambda}_2\cdot\nabla v_2=0 \tag{6}$$

$$\frac{\partial v_3}{\partial t}+\boldsymbol{\lambda}_3\cdot\nabla v_3=-\frac{1}{\rho}(n_{x_2}, -n_{x_1})\cdot\nabla p \tag{7}$$

$$\frac{\partial v_4}{\partial t}+\boldsymbol{\lambda}_4\cdot\nabla v_4=-c(n_{x_2}, -n_{x_1})\cdot\nabla v_3 \tag{8}$$

DOI: 10.1002/fld

where the characteristic variables are defined as

$$\mathrm{d}v_1 = -\hat{\mathbf{n}}\cdot\mathrm{d}\mathbf{u} + \frac{1}{\rho c}\mathrm{d}p, \quad \mathrm{d}v_2 = \mathrm{d}\rho - \frac{1}{c^2}\mathrm{d}p \tag{9}$$

$$\mathrm{d}v_3 = (n_{x_2}, -n_{x_1})\cdot\mathrm{d}\mathbf{u}, \quad \mathrm{d}v_4 = \hat{\mathbf{n}}\cdot\mathrm{d}\mathbf{u} + \frac{1}{\rho c}\mathrm{d}p \tag{10}$$

and the vector characteristic velocities (eigenvalues)

$$\boldsymbol{\lambda}_1 = \mathbf{u} - c\hat{\mathbf{n}}, \quad \boldsymbol{\lambda}_2 = \mathbf{u}, \quad \boldsymbol{\lambda}_3 = \mathbf{u}, \quad \boldsymbol{\lambda}_4 = \mathbf{u} + c\hat{\mathbf{n}} \tag{11}$$

To avoid confusion, more details on multidimensional characteristics need to be explained here. As in the 1-D characteristic form, $\mathrm{d}v_i$ denotes the variation of v_i. However, in general, the differential Equations (9) and (10) for the characteristic variables are not fully analytically integrable, because ρ and c are not constants. Although the characteristic variables v_i are not always analytically defined, their variations $\mathrm{d}v_i$ are defined. This means that no ordinary differential equation governs the characteristic variable along the characteristic line or surface and, thus, one cannot simply integrate the ODE along the characteristic line or surface to obtain the characteristic variables. Therefore, the variations of the characteristic variables are considered and the coupled partial differential equations must be integrated instead.

To obtain the appropriate nonreflecting boundary conditions, the problem becomes how to analyze the four waves separately. It is easy to handle entropy, vorticity, and transport waves as discussed in Appendix A.3, because they are convected by the known velocity $\mathbf{u}$. In contrast, it is rather complicated to analyze the two acoustic waves. Actually, most of the spurious reflections stem from these two waves because it is difficult to mimic these two physical waves at the artificial boundaries. Theoretically, the local direction of the acoustic waves can be determined by solving $(n_{x_2}, -n_{x_1})\cdot\nabla v_3 = 0$. However, in practice, this process introduces complications and, for general flows, it is impossible to find any direction to satisfy the condition $(n_{x_2}, -n_{x_1})\cdot\nabla v_3 = 0$. The source term can be rewritten in the quadratic form

$$\begin{aligned}(n_{x_2}, -n_{x_1})\cdot\nabla v_3 &= \frac{\partial u_1}{\partial x_1}n_{x_2}^2 - \left(\frac{\partial u_2}{\partial x_1} + \frac{\partial u_1}{\partial x_2}\right)n_{x_1}n_{x_2} + \frac{\partial u_2}{\partial x_2}n_{x_1}^2 \\ &= [n_{x_2} \;\; n_{x_1}]\underbrace{\begin{bmatrix}\varepsilon_{11} & -\varepsilon_{12}\\ -\varepsilon_{21} & \varepsilon_{22}\end{bmatrix}}_{\eta_{ij}}\begin{bmatrix}n_{x_2}\\ n_{x_1}\end{bmatrix}\end{aligned} \tag{12}$$

where the shear-strain rate is defined as $\varepsilon_{ij} = \frac{1}{2}(\partial u_i/\partial x_j + \partial u_j/\partial x_i)$. Note that both tensors η_{ij} and ε_{ij} are symmetric and they share the same set of real eigenvalues. The symmetry also implies that there is a set of principal axes. The local direction of the acoustic waves can be determined only if the matrix has both positive and negative eigenvalues. However, for general flows, $(n_{x_2}, -n_{x_1})\cdot\nabla v_3$ is the positive definite or negative definite if the eigenvalues of the matrix are positive or negative, respectively. This means that the shear-strain rate contracts or expands in both the principal axes. Therefore, for general compressible flows it is not always possible to determine the local direction of the acoustic waves that completely eliminates the source terms.

Note that all the scalar transport properties, such as vorticity, discussed in Appendix A.3, have relatively small reflection by using either the 1-D or the multidimensional characteristic

DOI: 10.1002/fld

boundary conditions. The reason is that the acoustic source term does not appear in their governing equations and, although there is spurious velocity reflection, the scalar properties are convected out of the computational domain with modified convection velocity. In contrast, the acoustic source term does appear in the governing equations of density, pressure, temperature, and velocity. Therefore, the LODI approach with inherent 1-D characteristics generates strong spurious reflections for them. So, the key to mimic the physical phenomena and minimize the spurious reflection from the artificial boundaries is to properly modify the source term $(n_{x_2}, -n_{x_1}) \cdot \nabla v_3$ and obtain the effective source term in addition to the multidimensional characteristic approach.

2.3. 2-D Characteristic boundary conditions

Without loss of generality, let us consider the right boundary condition at $x_1 = x_1^{\max}$. Since the normal unit vector $\hat{\mathbf{n}}$ is arbitrary, a simple $\hat{\mathbf{n}} = (1, 0)$ can be reasonably chosen for the outflow boundary. This selection makes the formulation simple and identifying the incoming and outgoing waves easy. Then, the above formulations reduce to

$$\frac{\partial v_1}{\partial t} + \boldsymbol{\lambda}_1 \cdot \nabla v_1 = -c \frac{\partial u_2}{\partial x_2} \tag{13}$$

$$\frac{\partial v_2}{\partial t} + \boldsymbol{\lambda}_2 \cdot \nabla v_2 = 0 \tag{14}$$

$$\frac{\partial v_3}{\partial t} + \boldsymbol{\lambda}_3 \cdot \nabla v_3 = \frac{1}{\rho} \frac{\partial p}{\partial x_2} \tag{15}$$

$$\frac{\partial v_4}{\partial t} + \boldsymbol{\lambda}_4 \cdot \nabla v_4 = -c \frac{\partial u_2}{\partial x_2} \tag{16}$$

where

$$\mathrm{d}v_1 = -\mathrm{d}u_1 + \frac{1}{\rho c}\mathrm{d}p, \quad \mathrm{d}v_2 = \mathrm{d}\rho - \frac{1}{c^2}\mathrm{d}p, \quad \mathrm{d}v_3 = -\mathrm{d}u_2, \quad \mathrm{d}v_4 = \mathrm{d}u_1 + \frac{1}{\rho c}\mathrm{d}p \tag{17}$$

and the vector characteristic velocities (eigenvalues)

$$\boldsymbol{\lambda}_1 = (u_1 - c, u_2), \quad \boldsymbol{\lambda}_2 = (u_1, u_2), \quad \boldsymbol{\lambda}_3 = (u_1, u_2), \quad \boldsymbol{\lambda}_4 = (u_1 + c, u_2) \tag{18}$$

The left-hand sides of this characteristic form are the waves along the characteristics. The right-hand sides are the source terms. When dealing with the source terms, Thompson [15, 16] just put them into the equation without any modification.

Owing to the source terms, the characteristic variables may not be constant along characteristics. This means that for the incoming waves in the outflow boundary, $\lambda_1 \cdot \nabla v_1$ is nonzero for multidimensional flows and as a consequence cannot be determined, mainly because it comes from unavailable incoming waves. However, its effective contribution can be modeled with an optimal coefficient for the transverse term. Equivalently from the mathematical viewpoint, if $\lambda_1 \cdot \nabla v_1$ is set to zero as usual, only part of the source term $c\partial u_2/\partial x_2$ effectively contributes to the term $\partial v_1/\partial t$. Thus, in order to obtain appropriate nonreflecting boundary conditions, the source terms of the

DOI: 10.1002/fld

incoming acoustic wave must be partially damped as follows:

$$\frac{\partial v_1}{\partial t}+\boldsymbol{\lambda}_1\cdot\nabla v_1=-\beta_1^- c\frac{\partial u_2}{\partial x_2} \tag{19}$$

$$\frac{\partial v_2}{\partial t}+\boldsymbol{\lambda}_2\cdot\nabla v_2=0 \tag{20}$$

$$\frac{\partial v_3}{\partial t}+\boldsymbol{\lambda}_3\cdot\nabla v_3=\frac{1}{\rho}\frac{\partial p}{\partial x_2} \tag{21}$$

$$\frac{\partial v_4}{\partial t}+\boldsymbol{\lambda}_4\cdot\nabla v_4=-\beta_1^+ c\frac{\partial u_2}{\partial x_2} \tag{22}$$

Nonreflecting boundary conditions are obtained by setting the corresponding damping coefficient to unity for outgoing waves while for incoming waves, setting the corresponding damping coefficient to some value between zero and unity and the magnitudes of incoming waves to zero. This approach is consistent with the fact that only part of the source terms effectively contribute to the characteristic variables along the characteristics for incoming waves. Therefore, the key part of the proposed approach becomes how to set the damping coefficients for incoming waves. For the oblique plane acoustic waves, their optimal values are analyzed in details in Section 2.4 and numerically verified in Section 3.1. For general flows, their optimal values are estimated in Section 2.5 from a physical viewpoint and numerically tested in Section 3.2 for a flow around a cylinder with strong shedding vortices.

2.4. Acoustic plane wave analysis

All 1-D characteristic boundary conditions are exact for the normal waves. However, a strong reflection can be seen for the case of oblique waves due to the inherent 1-D wave modelling. For practical flow simulations, the method should have only slight reflection for a wide spectrum of angles of incidence. In this section, the plane wave propagation is analyzed in the context of the proposed scheme. Since, in this case, exact solutions exist for the physical domain, an exact β_1^- value for an angle of incidence and an optimal β_1^- value for a range of the angles of incidence can be obtained analytically. The rigorous analysis is used to demonstrate the critical roles that the multidimensional characteristics and optimal coefficients play in our approach. Without loss of generality, the right boundary at $x_1=x_1^{\max}$ is used to illustrate the analysis. For acoustic wave propagation problems, the acoustic wave dominance is assumed.

2.4.1. Exact solution in the physical domain. The governing equations of acoustic wave propagation problem in the physical domain can be derived by linearizing Equations (13)–(16) around the mean flow with velocity $(M,0)$, where $M<1$ is the inflow Mach number. The resulting linearized Euler equation is

$$\frac{\partial v_1}{\partial t}+(M-1,0)\cdot\nabla v_1=-\frac{\partial u_2}{\partial x_2} \tag{23}$$

$$\frac{\partial v_2}{\partial t}+(M,0)\cdot\nabla v_2=0 \tag{24}$$

DOI: 10.1002/fld

$$\frac{\partial v_3}{\partial t}+(M,0)\cdot\nabla v_3=\frac{\partial p}{\partial x_2} \tag{25}$$

$$\frac{\partial v_4}{\partial t}+(M+1,0)\cdot\nabla v_4=-\frac{\partial u_2}{\partial x_2} \tag{26}$$

where

$$\mathrm{d}v_1=-\mathrm{d}u_1+\mathrm{d}p,\quad \mathrm{d}v_2=\mathrm{d}\rho-\mathrm{d}p,\quad \mathrm{d}v_3=-\mathrm{d}u_2,\quad \mathrm{d}v_4=\mathrm{d}u_1+\mathrm{d}p \tag{27}$$

Note that all of these variables are perturbation quantities and the normalized local speed of sound $c=1$.

The plane acoustic wave has the exact solution of the general form

$$\rho=p,\quad u_1=\cos\theta p,\quad u_2=\sin\theta p \tag{28}$$

where the perturbation pressure p is an arbitrary function of η,

$$\eta=t-\hat{l}\cdot[\mathbf{x}-(M,0)t]=(1+M\cos\theta)t-\cos\theta x_1-\sin\theta x_2 \tag{29}$$

the unit vector $\hat{l}=(\cos\theta,\sin\theta)$ represents the plane wave propagation direction, $\theta\in[-\pi/2,\pi/2]$ or $[-90^\circ,90^\circ]$ is the angle of incidence for the outgoing wave, and $\mathbf{x}=(x_1,x_2)$ is the position vector. Note that this exact solution satisfies Equations (23)–(26) in the physical domain, which can be verified by directly substituting them into the linearized Euler equation.

2.4.2. Nonreflecting boundary conditions. For the artificial boundary at $x_1=x_1^{\max}$ in the computational domain, nonreflecting boundary conditions are solved. These nonreflecting boundary conditions come from the linearized Euler Equations (23)–(26) by just modifying the first equation representing a incoming wave. By setting the magnitudes of the incoming waves to zero, the first equation reduces to:

$$\frac{\partial v_1}{\partial t}+\beta_1^-\frac{\partial u_2}{\partial x_2}=0 \tag{30}$$

It has been mentioned that the exact solution satisfies Equations (24)–(26). However, the exact solution does not satisfy the modified equation for any incident angle if a specific β_1^- is used. Thus, the error arises from this modified equation. If these solutions satisfy the modified equation exactly, then nonreflecting boundary conditions yield the exact solution. Therefore, it is useful to analyze the modified equation for the exact solution.

2.4.3. Exact damping coefficient for an incident angle. Substituting the exact solution into the left-hand side of the modified equation yields

$$\frac{\partial v_1}{\partial t}+\beta_1^-\frac{\partial u_2}{\partial x_2}=A\frac{\mathrm{d}p}{\mathrm{d}\eta} \tag{31}$$

where the amplification factor

$$A(M,\beta_1^-,\theta)=(1-\cos\theta)(1+M\cos\theta)-\beta_1^-\sin^2\theta \tag{32}$$

DOI: 10.1002/fld

Note that the amplification factor A is symmetric with respect to θ, i.e. $A(M, \beta_1^-, -\theta) = A(M, \beta_1^-, \theta)$. In general, the amplification factor is not zero, which means the modified equation generates some error.

An exact damping coefficient can be found for a specific incident wave by solving $A = 0$. The corresponding exact damping coefficient becomes

$$\beta_1^- = \frac{(1-\cos\theta)(1+M\cos\theta)}{\sin^2\theta} = \frac{1+M\cos\theta}{1+\cos\theta} = M + \frac{1-M}{1+\cos\theta} \tag{33}$$

This implies that the exact damping coefficient is different for different angles of incidence of a plane wave with an arbitrary shape and that, for all angles of incidence $\theta \in [-\pi/2, \pi/2]$, $\beta_1^- \in [(1+M)/2, 1]$. This narrow band of the exact damping coefficient is verified in Figure 1 for different mean flows. The narrow band suggests that it is possible to choose a certain value in the middle of the range such that the error is minimized. Particularly, when M is large, the range is very narrow and thus the value can be easily determined.

For simplicity in the numerical simulation, a fixed damping coefficient β_1^- can be used for all incident angles. For this fixed value, it is useful to consider the corresponding magnitude of amplification factor A. Figure 2 shows the errors for respective $(M, \beta_1^-) = (0, 0.6), (0.2, 0.75), (0.6, 0.9)$, and $(0.8, 0.96)$ for different angles. It suggests that the error is very small in a very large range. For example, $(M, \beta_1^-) = (0, 0.6), (0.2, 0.75), (0.6, 0.9), (0.8, 0.96)$ gives good results for $[-60°, 60°]$, $[-70°, 70°]$, $[-80°, 80°]$, and $[-90°, 90°]$, respectively.

2.4.4. Optimal damping coefficient for a range of incidence angles. In some physical and numerical problems, most or all of the waves have angles of incidence between zero and a maximum value θ_m. It is sufficient to minimize reflections for these incident waves. To find the optimal damping

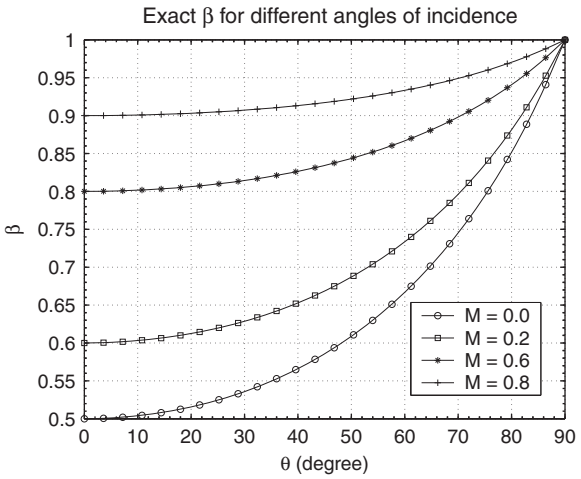

Figure 1. Exact β_1^- for different angles of incidence.

DOI: 10.1002/fld

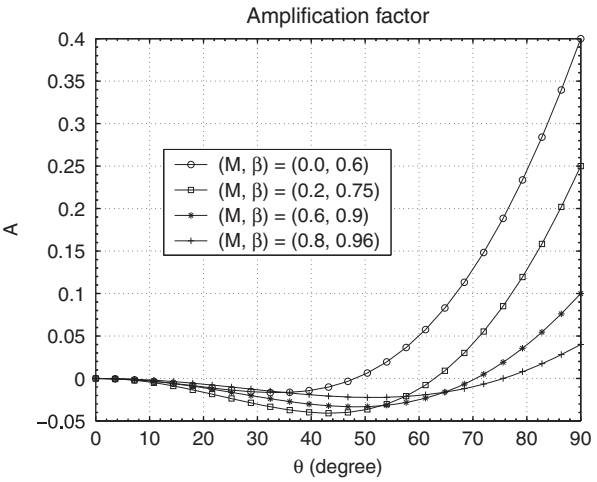

Figure 2. Amplification factor for different M and β_1^- values.

values, the following least-square error need to be minimized:

$$I(\beta_1^-, M, \theta_m) = \int_{-\theta_m}^{\theta_m} [(1-\cos\theta)(1+M\cos\theta) - \beta_1^- \sin^2\theta]^2 \,\mathrm{d}\theta$$
$$= 2\int_0^{\theta_m} [(1-\cos\theta)(1+M\cos\theta) - \beta_1^- \sin^2\theta]^2 \,\mathrm{d}\theta \tag{34}$$

where θ_m is a prescribed parameter. Taking the derivative $\partial I/\partial\beta_1^- = 0$ gives the corresponding optimal β_1^- value for this optimization problem

$$\beta_1^{-\mathrm{opt}}(M, \theta_m) = \frac{\int_0^{\theta_m}(1-\cos\theta)(1+M\cos\theta)\sin^2\theta\,\mathrm{d}\theta}{\int_0^{\theta_m}\sin^4\theta\,\mathrm{d}\theta} \tag{35}$$

which reduces to

$$\beta_1^{-\mathrm{opt}} = \frac{(4-M)\theta_m - 2\sin(2\theta_m) - \frac{8}{3}(1-M)\sin^3\theta_m + (M/4)\sin(4\theta_m)}{3\theta_m - 2\sin(2\theta_m) + \frac{1}{4}\sin(4\theta_m)} \tag{36}$$

The optimal β_1^- values for different angles and some selected M values are shown in the left column of Figure 3. The corresponding maximum amplification factor can be calculated as

$$A_{\max}(M, \theta_m) = \max_{\theta\in[-\theta_m,\theta_m]} |A(M, \beta_1^{-\mathrm{opt}}, \theta)| \tag{37}$$

The maximum amplification factor for different ranges of angles and for few selected M values are shown in the right column of Figure 3. The figure can be interpreted in the following two ways.

DOI: 10.1002/fld

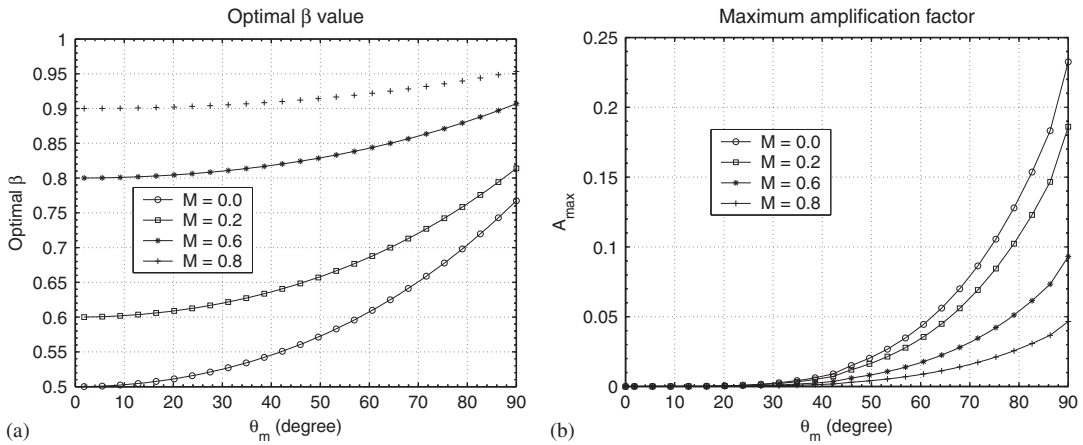

Figure 3. Optimal β_1^- value (a) and maximum amplification factor and (b).

Consider the situation that waves with angles of incidence between $-\theta_m$ and θ_m are of interest. As an example, $\theta_m = 60°$. Figure 3 can be interpreted using Figure 3(a) and (b) as an example for $M = 0$. From Figure 3(a), the selection of $\beta_1^{-\text{opt}} = 0.6$ can be found for $\theta_m = 60°$. This means that small errors are resulted for the reflected waves. Then look up Figure 3(b) for $\theta_m = 60°$ and find that the corresponding maximum amplification factor is less than 0.05. For $M = 0.2$, 0.6, and 0.8, the optimal $\beta_1^{-\text{opt}}$ values can be found to be 0.68, 0.84, and 0.92, respectively. The corresponding maximum amplification factor is 0.035, 0.018, and 0.008, respectively. These maximum errors may be sufficient for some practical multidimensional flow simulations.

Consider another situation that the maximum amplification factor is prescribed for accuracy. As an example, $A_{\max} = 0.05$. Figure 3 can be interpreted using Figure 3(a) and (b) as an example for $M = 0$. From Figure 3(b), $\theta_m = 60°$ can be found. Then look up Figure 3(a) for $\theta_m = 60°$ and find the optimal $\beta_1^{-\text{opt}} = 0.6$. For $M = 0.2$, 0.6, and 0.8, the maximum angles θ_m can be found to be approximately 68, 75, and 90°, respectively. The corresponding optimal $\beta_1^{-\text{opt}}$ values can be found to be 0.72, 0.87, and 0.953, respectively.

2.5. *General flow analysis*

Unlike the plane acoustic waves, the closed-form solution does not exist for arbitrary flows in general. This difficulty make it impossible to perform the similar rigorous analysis for arbitrary flows. However, for flows with hydrodynamic waves much stronger than acoustic waves, the optimal $\beta_1^{-\text{opt}} = u_1/c$ is proposed where $c = T^{1/2}$ is the normalized local speed of sound. This proposed value is based on analysis in physical viewpoint as follows and in addition on numerical simulations in Section 3.2.

2.5.1. Nonreflecting boundary conditions. Without loss of generality, the outflow boundary at $x_1 = x_1^{\max}$ is used to illustrate the analysis. The general flows are governed by Equations (13)–(16) in the physical domain. For the artificial boundary at $x_1 = x_1^{\max}$ in the computational domain, nonreflecting boundary conditions are solved. These nonreflecting boundary conditions come from

DOI: 10.1002/fld

the governing equations (13)–(16) by just modifying the first equation representing an incoming wave. For supersonic flows, Equations (13)–(16) do not need any modification. For subsonic flows, Equation (13) needs to be modified. By setting the magnitudes of the incoming wave to zero, Equation (13) is replaced by

$$\frac{\partial v_1}{\partial t} = -\beta_1^- c \frac{\partial u_2}{\partial x_2} \tag{38}$$

and the remaining three equations are untouched. The optimal damping coefficient in the modified equation needs to be set to minimize the spurious reflection.

A mathematically equivalent approach is to consider the sum and difference of the two acoustic wave Equations (16) and (38). The equivalent equations become

$$\frac{2}{\rho c}\frac{\partial p}{\partial t} = -(u_1+c)\frac{\partial u_1}{\partial x_1} - \frac{u_1+c}{\rho c}\frac{\partial p}{\partial x_1} - (1+\beta_1^-)c\frac{\partial u_2}{\partial x_2} - u_2\left(\frac{\partial u_1}{\partial x_2} + \frac{1}{\rho c}\frac{\partial p}{\partial x_2}\right) \tag{39}$$

$$2\frac{\partial u_1}{\partial t} = -(u_1+c)\frac{\partial u_1}{\partial x_1} - \frac{u_1+c}{\rho c}\frac{\partial p}{\partial x_1} - (1-\beta_1^-)c\frac{\partial u_2}{\partial x_2} - u_2\left(\frac{\partial u_1}{\partial x_2} + \frac{1}{\rho c}\frac{\partial p}{\partial x_2}\right) \tag{40}$$

Owing to the inherent difficulty of analysis for arbitrary flows, we perform the analysis for different flow regimes: $M \ll 1$ and $(1-M) \ll 1$. The rest of this section is used to give some physical argument for the estimation of the optimal value of β_1^-.

2.5.2. Lower Mach number flows. For compressible flows, the variations of pressure and velocity are of $O(M^2)$ and $O(M)$ [34], respectively. For lower Mach number flows, orders of all terms in Equation (39) can be analyzed. The terms $(u_1+c)\partial u_1/\partial x_1$ and $(1+\beta_1^-)c\partial u_2/\partial x_2$ are of $O(M)$ while the rest terms are of $O(M^2)$. Hence, the two leading terms $(u_1+c)\partial u_1/\partial x_1$ and $(1+\beta_1^-)c\partial u_2/\partial x_2$ need to balance each other.

Equations (1) and (6) give the relation

$$\frac{\partial u_2}{\partial x_2} = -\frac{\partial u_1}{\partial x_1} - \frac{1}{\rho c^2}\frac{Dp}{Dt} \approx -\frac{\partial u_1}{\partial x_1} \tag{41}$$

since Dp/Dt is of order $O(M^2)$. Therefore, the balance gives the optimal damping coefficient

$$\beta_1^- = u_1/c \tag{42}$$

As expected from this analysis, $\beta_1 = u_1/c$ gives good results for the lower Mach number region $M < 0.3$.

For a low Mach number flow, Yoo and Im [27] performed an asymptotic analysis, yielding the modified LODI boundary condition for the incoming wave

$$\frac{\partial v_1}{\partial t} = -Mc\frac{\partial u_2}{\partial x_2} \tag{43}$$

This approximation is consistent with the proposed optimal value of $\beta_1^- = u_1/c$. However, the analysis of Yoo and Im is still based on 1-D characteristics and, as a result, numerical simulations were performed only for a very lower Mach number $M = 0.05$. In this limit, our approach coincides with the approach of Yoo and Im. As a consequence, the results reported in Reference [27] could

DOI: 10.1002/fld

also serve as quantitative demonstration of the improvement of our approach in the low Mach number limit. On the other hand, for the high Mach number flows it is hard to differentiate the acoustic wave from flow field, which in turn could be modified by the spurious waves reflected from the computational boundaries. Therefore, it is hard or even impossible to provide unbiased quantitative measure of the spurious wave reflection for high Mach number flows.

2.5.3. High Mach number flows. For supersonic flows with $u_1/c>1$, Equations (13)–(16) do not need any modification. When $u_1/c=1$, they are still valid and Equation (39) with $\beta_1^-=u_1/c=1$ exactly describes the flow. Denote the corresponding exact solutions as those with $\hat{}$ and Equation (38) becomes

$$-\frac{\partial \hat{u}_1}{\partial t}+\frac{1}{\rho c}\frac{\partial \hat{p}}{\partial t}=-c\frac{\partial \hat{u}_2}{\partial x_2} \tag{44}$$

For transonic flows with $u_1/c\geqslant 0.7$ the variables can be decomposed as

$$u_1=\hat{u}_1+\varepsilon u_1^*+O(\varepsilon^2),\quad u_2=\hat{u}_2+\varepsilon u_2^*+O(\varepsilon^2),\quad p=\hat{p}+\varepsilon p^*+O(\varepsilon^2) \tag{45}$$

where $\varepsilon\ll 1$. Substituting Equation (45) into Equation (38) yields

$$-(1-\beta_1^-)c\frac{\partial \hat{u}_2}{\partial x_2}=\varepsilon\frac{\partial u_1^*}{\partial t}-\frac{\varepsilon}{\rho c}\frac{\partial p^*}{\partial t}-\varepsilon\beta_1^- c\frac{\partial u_2^*}{\partial x_2} \tag{46}$$

Since the right-hand side is of $O(\varepsilon)$, $1-\beta_1^-=O(\varepsilon)$, which suggests that either $\beta_1^-=u_1/c$ or $\beta_1^-=M$ can be used for the damping coefficient.

2.5.4. General subsonic flows. The above two cases suggest that $\beta_1^-=u_1/c$ can be used as optimal damping coefficient for general subsonic flows. This assumption was verified only numerically as discussed in Section 3.2. In addition, some physical insights can be obtained by considering an alternative form of Equations (39) and (40)

$$\frac{2}{\rho c}\frac{\partial p}{\partial t}=-(u_1-\beta_1^- c)\frac{\partial u_1}{\partial x_1}-(u_1+c)\frac{1}{\rho c}\frac{\partial p}{\partial x_1}-u_2\left(\frac{\partial u_1}{\partial x_2}+\frac{1}{\rho c}\frac{\partial p}{\partial x_2}\right)+\frac{1+\beta_1^-}{\rho c}\frac{\mathrm{D}p}{\mathrm{D}t} \tag{47}$$

$$2\frac{\partial u_1}{\partial t}=-(u_1+\beta_1^- c)\frac{\partial u_1}{\partial x_1}-(u_1+c)\frac{1}{\rho c}\frac{\partial p}{\partial x_1}-u_2\left(\frac{\partial u_1}{\partial x_2}+\frac{1}{\rho c}\frac{\partial p}{\partial x_2}\right)+\frac{1-\beta_1^-}{\rho c}\frac{\mathrm{D}p}{\mathrm{D}t} \tag{48}$$

where $\mathrm{D}p/\mathrm{D}t\approx 0$ for convection dominant flows. The choice $\beta_1^{-\mathrm{opt}}=u_1/c$ makes acoustic or source terms partially annihilating each other. When $c\approx 1$, $\beta_1^-=u_1$ can be used. For simplicity, the mean flow Mach number M can be used for β_1^-. However, the numerical solutions in Section 3 demonstrate that $\beta_1^-=u_1/c$ gives better results.

For low Mach number flows, the proposed approach and that in Reference [27] coincide and, not surprisingly, result in the same optimal coefficient. For general Mach number flows, however, it is impossible to derive an optimal coefficient of the form $\beta_1^-=M$ using the methodology reported in Reference [27]. This is clear from the fact that, as already pointed out in Section 3.2 of Reference [27], the approach of Yoo and Im is not ideal for high Mach number flow cases. They also used $\beta_1^-=u_1$ in some test cases. However, it is only a simple extrapolation from the low Mach number case. As explained before, this coefficient does not work in high Mach number limit in the

DOI: 10.1002/fld

approach of Yoo and Im and, thus, cannot be derived using any rigorous reasoning. In contrast, in the proposed approach, the dumping coefficient $\beta_1^- = u_1/c$ is derived for arbitrary Mach number and is consistent with the physics of general flows.

Note that the separation of the two cases is a drawback of our approach. However, in many applications, there is a vast disparity in the magnitude of acoustic waves and convective waves. For these cases it is sufficient to suppress the convective wave reflections optimally while simultaneously the acoustic wave reflections partially by using $\beta_1^- = u_1/c$. For example, in the outflow boundary of flows around a cylinder, $\beta_1^- = u_1/c$ is sufficient for suppressing two kinds of wave reflections simultaneously. Note that even for the latter partially suppressed part, the proposed approach with $\beta_1^- = u_1/c$ outperforms the LODI approach, which ignores the transverse term and is equivalent to our approach using $\beta_1^- = 0$. The error for the acoustic part can be estimated as follows. If we use $\beta_1^- = M \approx u_1$, the amplification factor reduces to $A = (1 - \cos\theta)(1 - M)$. This suggests that we get good results for acoustic waves with small incident angles with any mean flows. However, for acoustic waves with large incident angles, $\beta_1^- = M \approx u_1$ gives accurate results only when u_1 is close to 1.

On the other hand, if very accurate solutions are needed for acoustic wave dominated or pure acoustic flows, we have to use the corresponding coefficients for acoustic wave propagations. One example is the bottom and top boundaries of flows around a cylinder. It should be noted that the approach in References [26] and [27], which works for hydrodynamic wave dominated low Mach number flows, generates strong reflections for acoustic wave dominated flows. However, it may be possible to find a unified approach for both the waves by considering optimal oblique wave propagation directions. This is under investigation and further work will be described in future papers.

3. RESULTS AND DISCUSSION

Two benchmark problems are tested for the multidimensional characteristics-based nonreflecting boundary conditions. One is the acoustic wave propagation problem with various angles of incidence. The other is the flow around a cylinder. The classical LODI approach generates strong reflections for both the problems. The two benchmark problems are used to illustrate the capabilities of the multidimensional characteristics-based nonreflecting boundary conditions to minimize the spurious wave reflection from the artificial boundaries for complex multidimensional flows.

3.1. Cylindrical acoustic waves

The acoustic benchmark problem is the free propagation of the cylindrical acoustic waves generated by localized acoustic sources. This problem is chosen because oblique waves with various angles of incidence propagate out of the computational domain. The problems of acoustic propagation out of the computational domain were considered for the *Second Computational Aeroacoustics* workshop on Benchmark Problems [35]. In contrast to most of the methods used in the workshop, which solved the linearized Euler equations, here the compressible Navier–Stokes equations are solved. For the Euler equations, the benchmark problems have exact analytical solutions [36]. The compressible Navier–Stokes equations are solved for an acoustic Reynolds number $Re_a = 10^5$ with the multidimensional nonreflecting boundary conditions. The time accurate direct numerical

DOI: 10.1002/fld

simulation (DNS) results for the field in the computational domain are compared with the analytical solution.

The cylindrical acoustic benchmark problem is simulated in a rectangular domain $\Omega=[-2,2]\times[-4,4]$, which is relatively very small so that the simulation is efficient. The initial conditions are localized pressure perturbations of the Gaussian distribution

$$p'=10^{-3}\exp\left[-\ln(2)\left(\frac{x^2+y^2}{0.04}\right)\right] \tag{49}$$

to the spatially uniform field. The corresponding initial conditions for the conservative variables are of the form

$$\rho=1+p', \quad e=\frac{1}{\gamma(\gamma-1)}+\frac{p'}{\gamma-1}, \quad m_1=0, \quad m_2=0 \tag{50}$$

Owing to the initial perturbations, a cylindrical acoustic wave forms and propagates toward the boundaries, which should ideally be transparent to the oblique acoustic waves with various angles of incidence. The solutions for this benchmark problem are shown in Figures 4–6. To highlight the difference among the numerical simulations, the same scales are used for Figures 4 and 5.

Figure 4 shows the numerical simulations of the cylindrical acoustic wave snapshots of the perturbation pressure for $\beta_1^-=0.6$ at three times $t=1.0$, $t=3.0$, and $t=4.0$. The results show that these new boundary conditions are appropriate for the oblique acoustic waves, because the oblique acoustic waves, with various angles of incidence, can propagate through the artificial boundaries without reflections. Figure 6, the time history for the point $(-2,2)$ shows that the time accurate DNS results match very well with the analytical solutions. The numerical simulations for the value $\beta_1^-=0.6$ are in good agreement with the analytical optimal value for the oblique acoustic waves in Section 2.4.

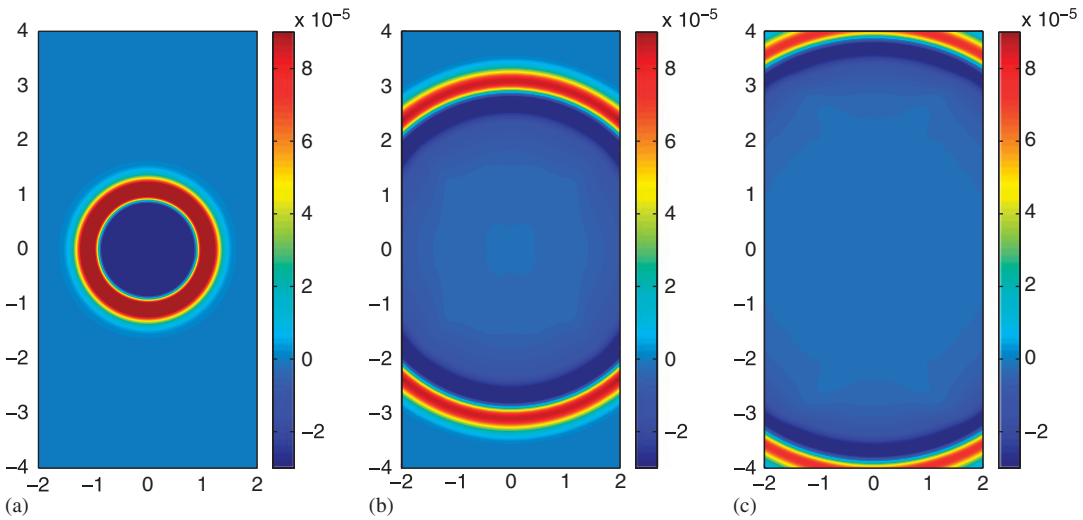

Figure 4. Time history of cylindrical acoustic wave propagation for $\beta_1^-=0.6$: (a) $t=1.0$; (b) $t=3.0$; and (c) $t=4.0$.

DOI: 10.1002/fld

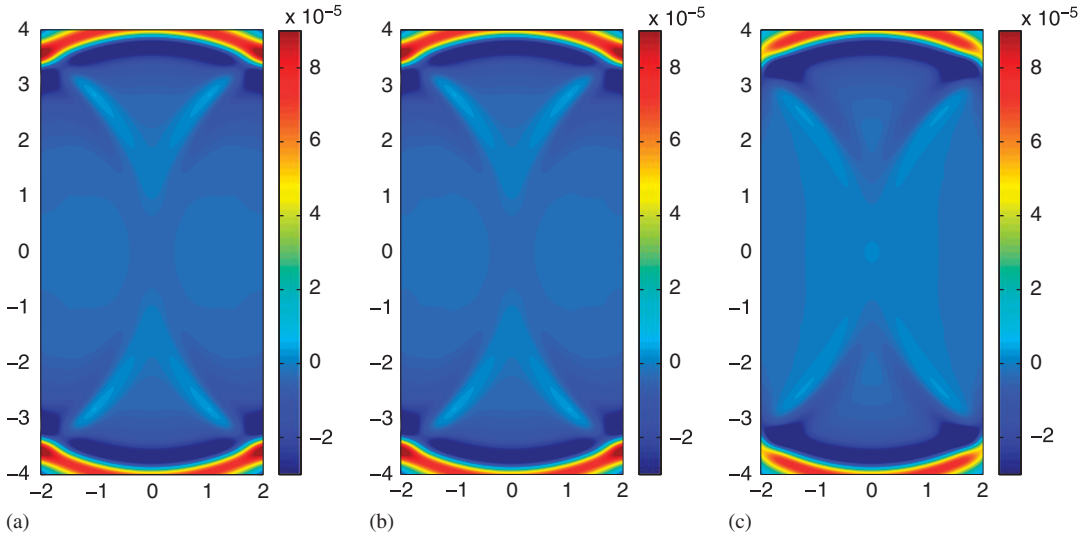

Figure 5. Cylindrical acoustic wave propagation: (a) LODI ($t=4.0$); (b) $\beta_1^- = 1.0$ ($t=4.0$); and (c) $\beta_1^- = 0.0$ ($t=4.0$).

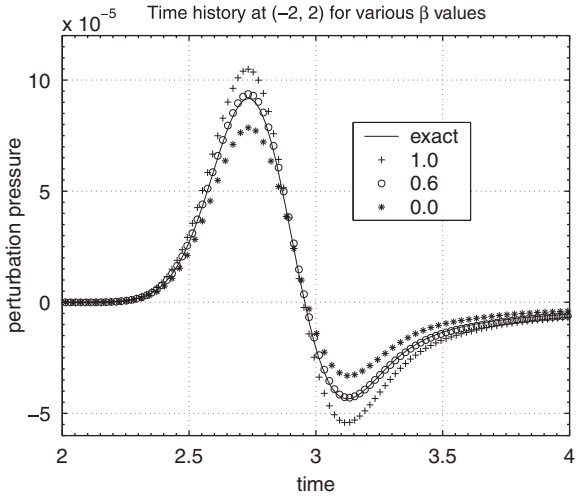

Figure 6. Time history for the point $(-2, 2)$.

Figure 5 shows the cylindrical acoustic wave snapshots of the perturbation pressure for the LODI approach, $\beta_1^- = 1.0$, and $\beta_1^- = 0.0$ at the same time $t=4.0$ as that for the last figure in Figure 4. All of the three cases have strong acoustic wave reflections from the artificial boundaries for the oblique waves. The reflected acoustic waves either strengthen or weaken the original acoustic waves near the artificial boundary and propagate into the computational domain to pollute the solutions. The results show considerable improvement of the multidimensional characteristic

DOI: 10.1002/fld

boundary conditions at $\beta_1^- = 0.6$ over the classical LODI approach. For the two β_1^- values 1.0 and 0.0, it is interesting that they have different phase errors with positive and negative signs, which can also be obviously observed from Figure 6. In Figure 6, the numerical solutions for $\beta_1^- = 0.6$, which is between $\beta_1^- = 0.0$ and $\beta_1^- = 1.0$, are transparent to the oblique waves and are in good agreement with the exact solutions.

3.2. Flow around cylinder

In the second benchmark problem, the 2-D compressible viscous flow around the cylinder is considered. This problem is chosen because strong vortices, generated behind the cylinder, are convected downstream and cross the artificial boundaries. The physical flow pattern is that all the properties, such as pressure, density, temperature, velocity, and vorticity, are convected downstream without any reflection from the outflow boundary. Then, the numerical simulations can be compared with the physical flows.

The previous work [13, 19, 37, 38] considered the outflow boundary conditions for the problem that compressible vortices cross the boundary. The LODI and other approaches generate strong pressure reflections and distortion without vorticity reflection. Prosser [24] applied the improved LODI approach to obtain slight pressure reflection and distortion for very low Mach number flows, when vortices cross the boundary. It is not a surprise that both 1-D and multidimensional characteristic boundary conditions do not generate the spurious reflection for vorticity. The reason is that vorticity is a transport variable convected downstream and the acoustic source term does not appear in its governing equation. Although there is spurious velocity reflection, vorticity is convected out of the computational domain with modified convection velocity. The details are discussed in Section 2.2 and Appendix A.3. For the outflow boundaries, Colonius [4] pointed out that some of the buffer techniques are presently the most accurate approaches. One of them is the Freund's zonal approach [11].

The cited previous studies did not consider the cases where multidimensional effects exist without vortices crossing the outflow boundary. Also, they only discussed the vorticity propagation and did not consider the velocity reflection. In this benchmark problem, the case with multidimensional effects, with/without vortex crossing, at the outflow boundary and all properties of velocity, pressure, density, temperature, and vorticity are studied. Thus, the goal is to mimic the physical outflow boundary to obtain the appropriate nonreflecting boundary conditions, which are transparent to all the properties. In the numerical simulations, the Brinkman penalization method for the compressible flows [39, 40] is applied for the cylinder.

3.2.1. Flow at $M = 0.2$. The 2-D compressible viscous flow around the cylinder at the Reynolds number $Re_a = 10^3$ and inflow Mach number $M = 0.2$ are considered. The flow is simulated in a domain $\Omega = [-5, 10] \times [-5, 5]$ with the DNS method for the compressible Navier–Stokes equations. The numerical solutions for this benchmark problem are shown in Figures 7–12 for the three cases: $\beta_1^- = M$, LODI, and $\beta_1^- = 0.6$ with strong multidimensional effects, with/without vortex crossing, at the outflow boundary at $x_1 = 10$ where strong multidimensional effects exist. The fields of vorticity ω, transverse velocity u_2, pressure p, and temperature T are shown for each case. To highlight the difference among the numerical simulations, the same scales are used for all three cases.

First, let us consider the case $\beta_1^- = 0.2$ using the multidimensional characteristic boundary conditions. Figure 7 is the instance that a vortex is crossing the outflow boundary. Figure 10 is the instance

DOI: 10.1002/fld

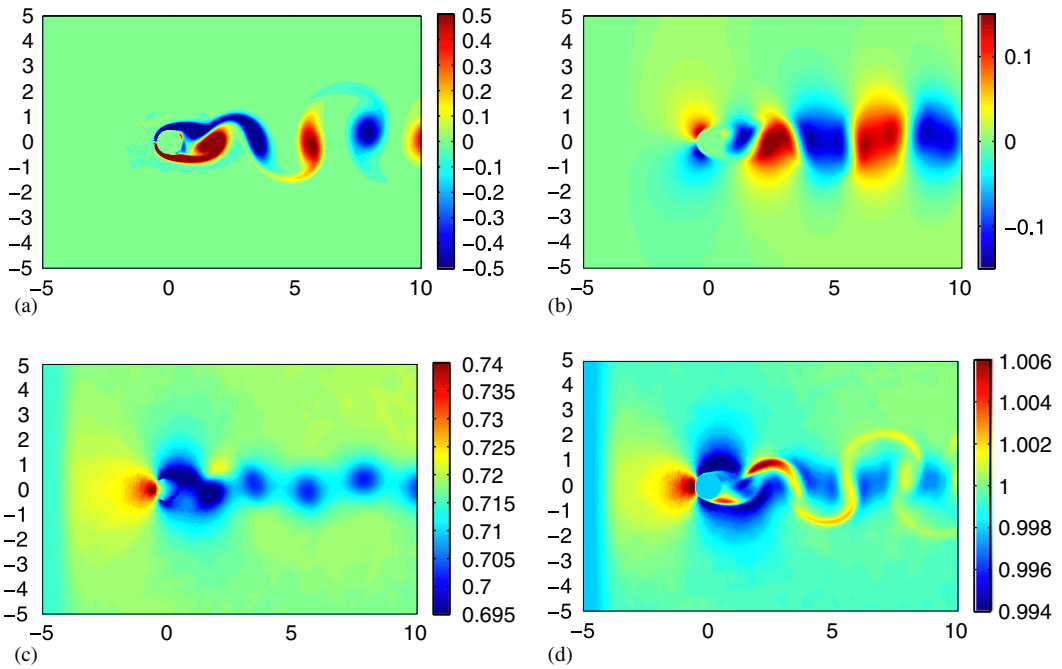

Figure 7. $\beta_1^- = 0.2$ for $M = 0.2$: profiles for (a) ω; (b) u_2; (c) p; and (d) T.

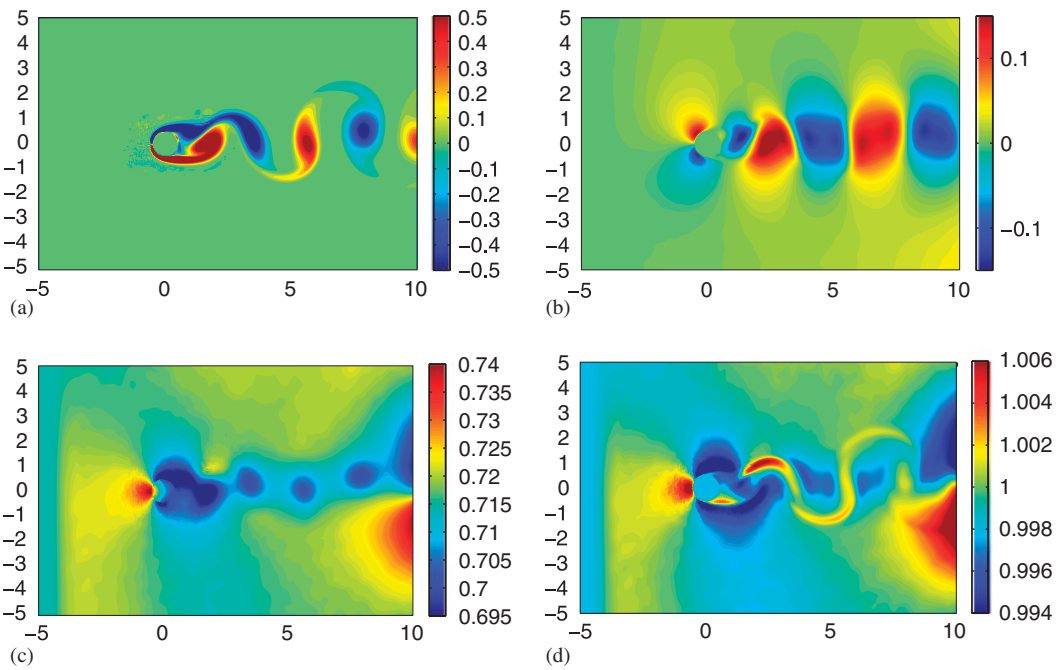

Figure 8. LODI for $M = 0.2$: profiles for (a) ω; (b) u_2; (c) p; and (d) T.

DOI: 10.1002/fld

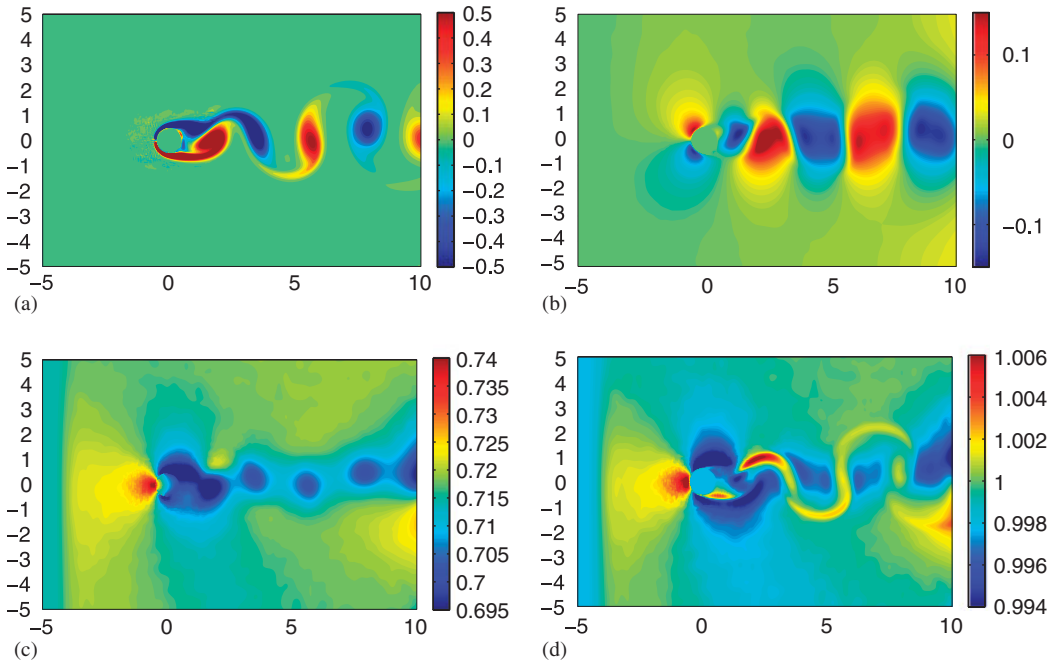

Figure 9. $\beta_1^- = 0.6$ for $M = 0.2$: profiles for (a) ω; (b) u_2; (c) p; and (d) T.

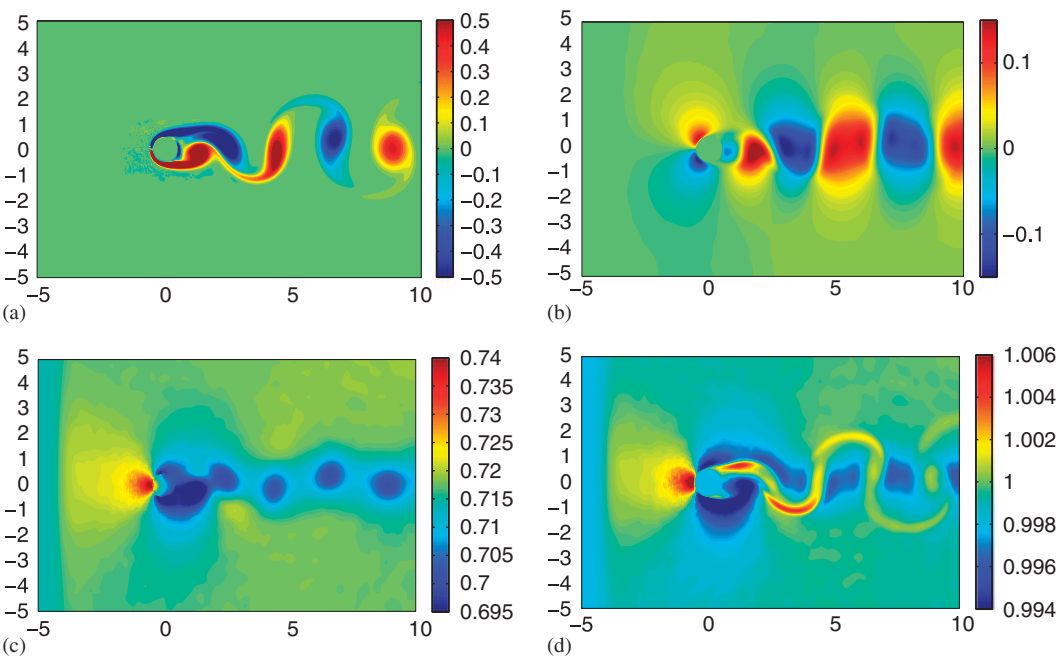

Figure 10. $\beta_1^- = 0.2$ for $M = 0.2$: profiles for (a) ω; (b) u_2; (c) p; and (d) T.

DOI: 10.1002/fld

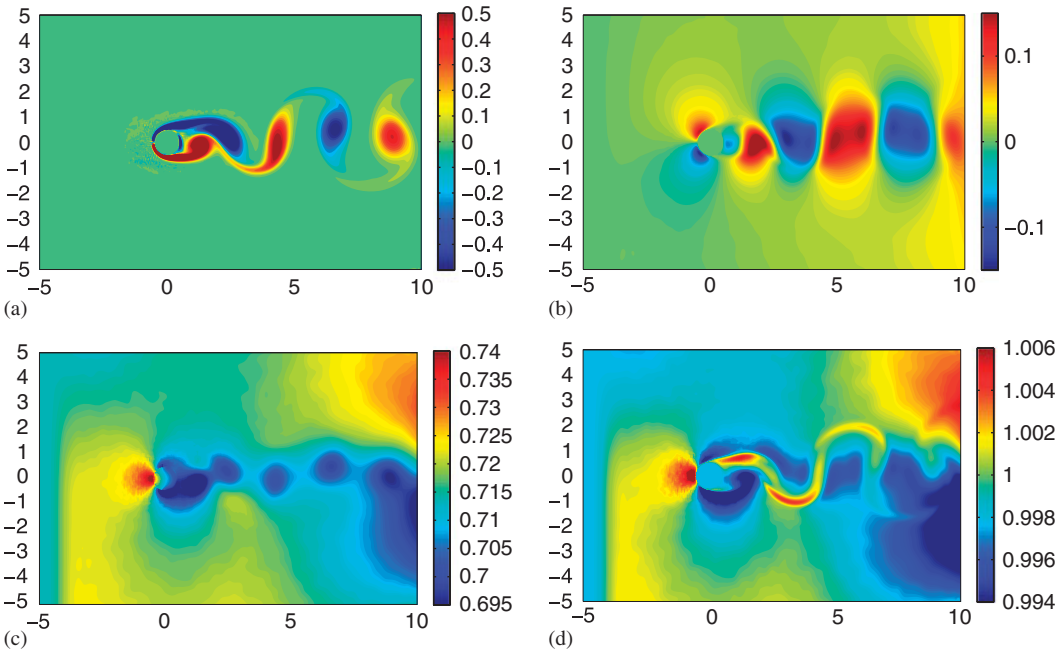

Figure 11. LODI for $M=0.2$: profiles for (a) ω; (b) u_2; (c) p; and (d) T.

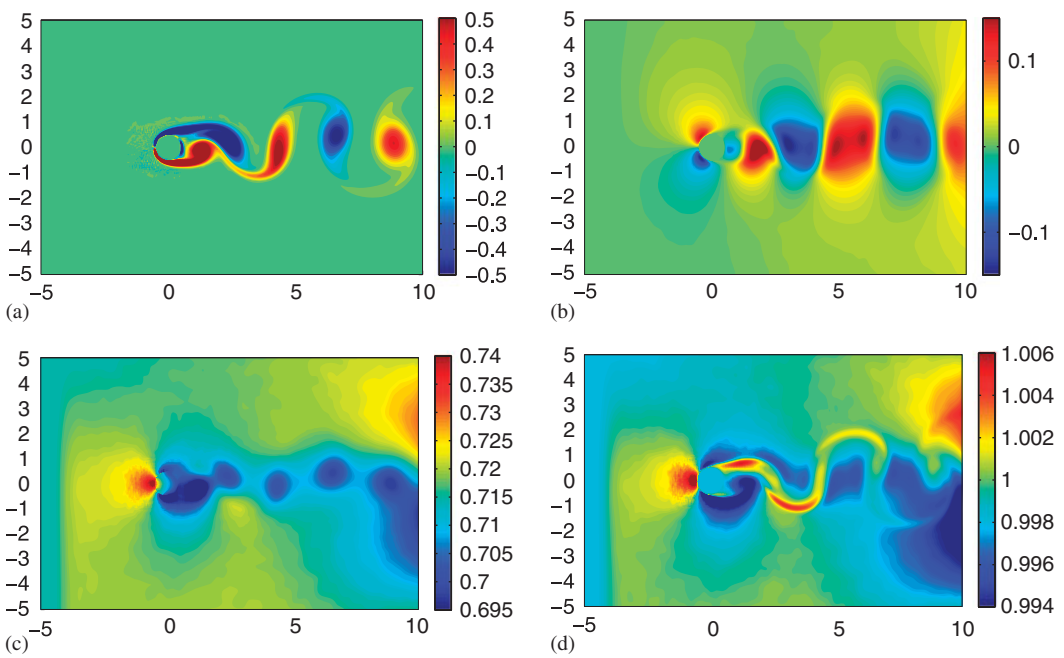

Figure 12. $\beta_1^- = 0.6$ for $M=0.2$: profiles for (a) ω; (b) u_2; (c) p; and (d) T.

DOI: 10.1002/fld

that a vortex already crossed the outflow boundary, and another vortex is approaching the outflow boundary. The numerical simulations show that the multidimensional characteristic boundary conditions with $\beta_1^- = 0.2$ are transparent to the pressure, density, temperature, and velocity, as well as vorticity. For this case, all profiles of the pressure, vortex, velocity, and temperature have not been distorted by the artificial boundary. Thus, this case has appropriate nonreflecting boundary conditions for a complex multidimensional flow. As a consequence, these solutions can be used as the reference for the other two cases. Any difference from the solutions for $\beta_1^- = 0.2$ is generated due to the reflection from the outflow boundary.

Second, let us consider the LODI case to find the difference between the 1-D characteristic approach and the multidimensional characteristic approach. Figure 8 is the instance that a vortex is crossing the outflow boundary. Figure 11 is the instance that a vortex has already crossed the outflow boundary and another vortex is approaching the outflow boundary. The figures show that, whether a vortex crosses the outflow boundary or not, the LODI approach generates stronger spurious pressure, density, temperature, and velocity reflection from the artificial outflow boundary, although only slight vorticity reflection is observed. Two strong spuriously generated pressure spots are observed at the outflow boundary, and the pressure spots are totally distorted. After the spurious acoustic waves are generated, they are observed to propagate upstream and contaminate the numerical solutions. The reason for the strong reflections for the LODI approach is that this approach uses the inherent 1-D characteristic modelling, but in fact the complex multidimensional flow structures and strong complicated multidimensional effects exist at the outflow boundary.

Finally, let us consider the case $\beta_1^- = 0.6$ to find the role of the damping coefficient. Figure 9 is the instance that a vortex is crossing the outflow boundary. Figure 12 is the instance that a vortex already crossed the outflow boundary, and another vortex is approaching the outflow boundary. The figures show that whether a vortex crosses the outflow boundary or not, spurious pressure, density, temperature, and velocity reflection are generated from the artificial outflow boundary, although only slight vorticity reflection is observed. Two strong spuriously generated pressure spots are observed at the boundary, and the pressure spots are totally distorted. After the spurious acoustic waves are generated, they are observed to propagate upstream and contaminate the numerical solutions. Although the reflections are similar to those for the LODI case, here they are weaker, which suggests that the proposed approach improves the LODI approach even using under-damping effects. The reason for the strong reflections is that this case uses under-damping effects when only part of the source terms effectively contribute to the characteristic variables along the characteristics. On the other hand, reflections can be observed for the over-damping cases, for example, $\beta_1^- = 0.0$.

In summary, $\beta_1^- = M$ minimizes the spurious wave reflection from the outflow boundary. This significantly improves the LODI approach. Even using under-damping and over-damping coefficients, the proposed approach improves the LODI approach. However, it is important to set proper damping effects for the source terms.

3.2.2. Flow at $M = 0.6$. In order to verify the optimal damping coefficient $\beta_1^- = u_1/c$ for arbitrary flows, the 2-D compressible viscous flow around the cylinder at the Reynolds number $Re_a = 400$ and another inflow Mach number $M = 0.6$ is considered. The flow is simulated in a domain $\Omega = [-5, 10] \times [-5, 5]$ with the DNS method for the compressible Navier–Stokes equations. Since it has already been shown that the proposed approach improves the LODI approach, this test

DOI: 10.1002/fld

problem considers the proper damping coefficient for a different inflow Mach number. The flow with strong multidimensional effects at the artificial outflow boundary is simulated for three cases: $\beta_1^- = u_1/c$, $\beta_1^- = 0.2$, and $\beta_1^- = M$. Numerical simulations of the fields of steamwise velocity u_1, transverse velocity u_2, pressure p, temperature T, and vorticity ω at an instantaneous time are shown in Figures 13–14. To highlight the difference among the numerical simulations, the same scales are used.

It is important to note that at the outflow boundary the streamwise velocity u_1 has a wide range of values, $u_1 \in [0.35, 0.8]$, as seen in Figure 13(a) for the case $\beta_1^- = u_1/c$. Thus, it is critical to set the proper damping coefficient in order to minimize spurious reflections. Based on results from analysis, $\beta_1^- = u_1/c$ is expected to minimize reflections. $\beta_1^- = M$, which is in the middle of the range, is expected to generate weak reflections. $\beta_1^- = 0.2$, which deviates from u_1, is expected to generate stronger reflections. Vorticity fields are shown in Figures 15(a) and 14(a). The results verify once again that the reflections are minimized for all cases. Vertical velocity fields are shown in Figures 13(b), 15(b), and 14(b). The results show that the reflections are minimized for all cases. Next, consider pressure and temperature fields for the three cases.

First, let us consider the case $\beta_1^- = u_1/c$ using the multidimensional characteristic boundary conditions in Figure 13. Note that the acoustic waves in the region around $x_1 < 2$ are generated by the unsteady shear boundary flow around the cylinder. They are not the spurious reflection from the artificial boundaries and thus they are unrelated to the proposed approach. The numerical simulations show that the multidimensional characteristic boundary conditions with $\beta_1^- = u_1/c$ are transparent to the pressure, density, temperature, and velocity, as well as vorticity. For this

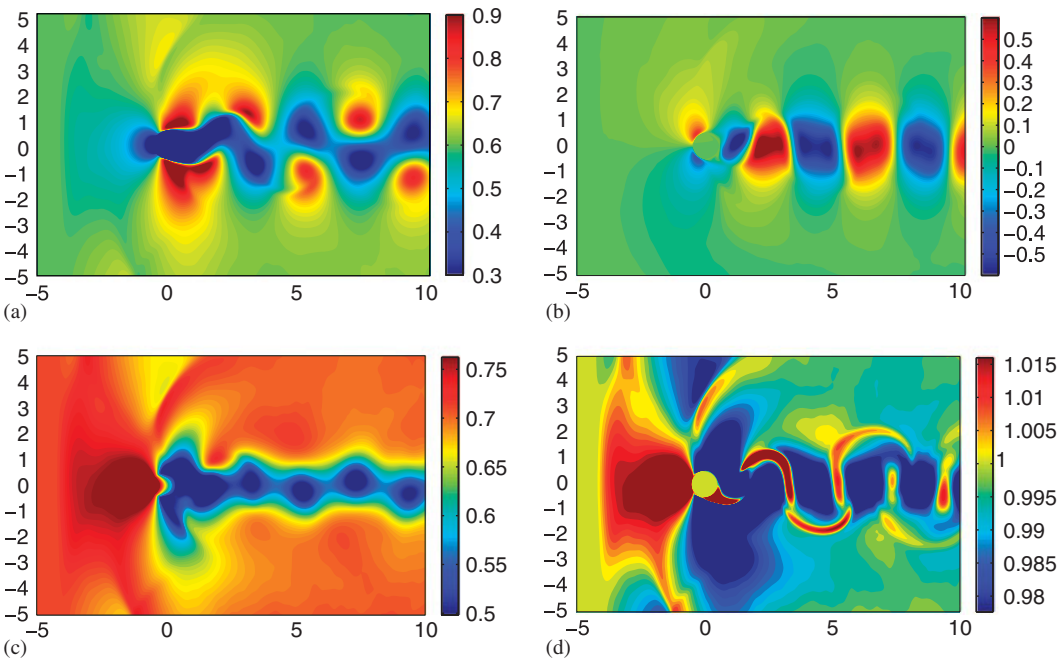

Figure 13. $\beta_1^- = u_1/c$: profiles for (a) u_1; (b) u_2; (c) p; and (d) T for $M = 0.6$.

DOI: 10.1002/fld

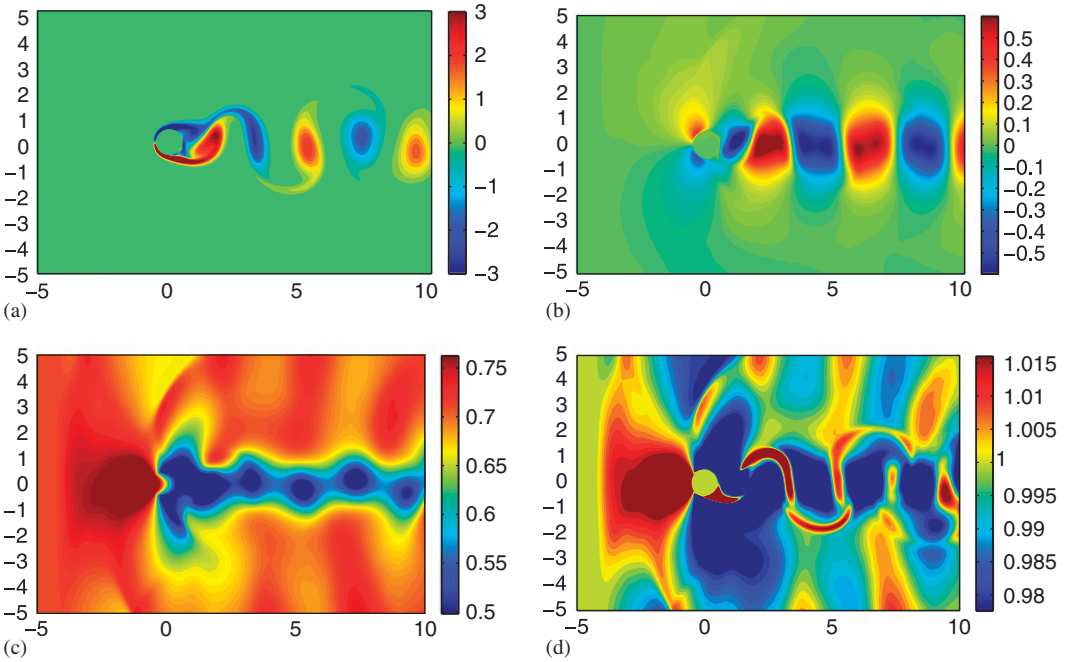

Figure 14. $\beta_1^- = 0.6$: profiles for (a) ω; (b) u_2; (c) p; and (d) T for $M = 0.6$.

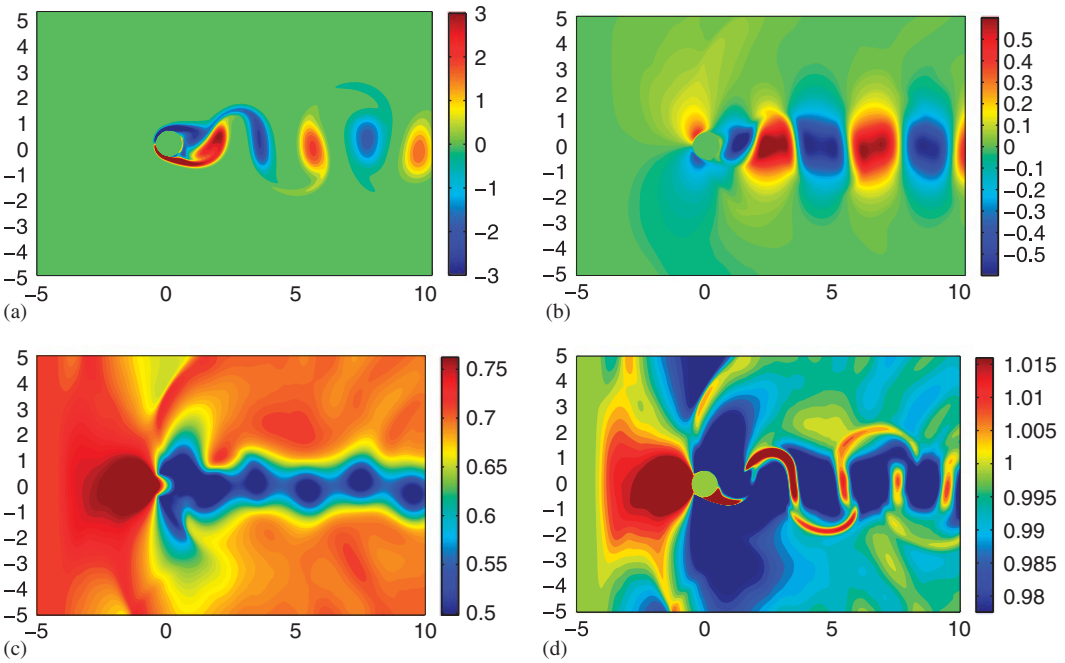

Figure 15. $\beta_1^- = 0.2$: profiles for (a) ω; (b) u_2; (c) p; and (d) T for $M = 0.6$.

DOI: 10.1002/fld

case, all profiles of the pressure, vortex, velocity, and temperature have not been distorted by the artificial boundary. Thus, this case has appropriate nonreflecting boundary conditions for a complex multidimensional flow. As a consequence, these solutions can be used as the reference for the other two cases. Any difference from the solutions for $\beta_1^- = u_1/c$ is generated due to the reflection from the artificial outflow boundary.

Second, let us consider the case $\beta_1^- = 0.2$ in Figure 15 and compare it with the case $\beta_1^- = u_1/c$. The figures show that this over-damping case generates strong spurious pressure, density, and temperature reflection from the artificial outflow boundary. After the spurious acoustic waves are generated, they are observed to propagate upstream and strongly contaminate the numerical solutions. The reason for the strong reflections is that this case uses over-damping effects when only part of the source terms effectively contribute to the characteristic variables along the characteristics.

Finally, let us consider the case $\beta_1^- = M$ in Figure 14. The figures show that this case generates weak spurious pressure, density, and temperature reflection from the artificial outflow boundary. After the spurious acoustic waves are generated, they are observed to propagate upstream and weakly contaminate the numerical solutions. Although the reflection patterns are similar to those in the case $\beta_1^- = 0.2$, here they are much weaker. This result verifies that it is important to set the proper damping effects for the source terms.

The numerical simulations confirm that the multidimensional characteristics are critical for the complex multidimensional flows. They also verify that the acoustic source term $(n_{x_2}, -n_{x_1}) \cdot \nabla v_3$ and its damping coefficient β_1^- play a very important role. On the one hand, all the transport properties discussed in Appendix A.3, whose governing equations do not have the acoustic source term, have relatively small reflection by using either the 1-D or the multidimensional characteristic boundary conditions. The reason is that the acoustic source term does not appear in their governing equations and, although there is spurious velocity reflection, the scalar properties are convected out of the computational domain with modified convection velocity. On the other hand, all the properties, such as density, pressure, temperature, and velocity, whose governing equations have the acoustic source terms have strong spurious reflections from the artificial boundaries. The good results of the new approach can be attributed to two factors. One is that the multidimensional characteristics better approximate the evolution of multidimensional flow structures and capture the complex multidimensional effects. The other is that the damping coefficient for the source term mimics the source terms appropriately for the physical phenomena. The optimal damping coefficient is suggested to use $\beta_1^- = u_1/c$, while $\beta_1^- = M$ also gives good results.

4. CONCLUSION

Nonreflecting boundary conditions based on nonlinear multidimensional characteristics has been proposed for 2- and 3-D compressible Navier–Stokes equations with/without scalar transport equations. In contrast to the approaches of Prosser [24, 25] and Im *et al.* [26, 27] in the context of 1-D characteristics for low Mach number flows, the proposed method is valid for general flows in addition to acoustic waves. Our approach is based on the rigorous mathematical analysis for general flows, which is consistent with the flow physics. The definition of characteristic wave amplitudes comes from the rigorous multidimensional characteristic analysis.

The source terms of the incoming acoustic wave are partially damped to model the effective contribution of the incoming waves. The acoustic plane wave analysis has been performed to obtain the optimal damping coefficient for acoustic problems. The optimal value is also estimated

DOI: 10.1002/fld

for general flows from a physical viewpoint. This model is consistent with the physics of flows and transport properties. Therefore, this new approach significantly minimizes the spurious wave reflections of pressure, density, temperature, and velocity as well as vorticity from the artificial boundaries, where strong multidimensional flow effects exist. The proposed method is simple, robust, and numerically accurate. This numerical accuracy is crucial for the computational aero-acoustic problems, whose quality of numerical simulations is very sensitive to the appropriate artificial boundary conditions. The proposed method is tested on two benchmark problems of cylindrical acoustic waves propagation and the wake flow. These numerical simulations yield accurate results and verify that the method substantially improves the 1-D characteristics-based nonreflecting boundary conditions for the complex multidimensional flows.

APPENDIX A

A.1. 2-D characteristic boundary conditions in primitive and conservative variables

For the x_1 boundaries, nonreflecting boundary conditions in the characteristic form, Equations (19)–(22), can be rewritten in the primitive variable form

$$\frac{\partial \rho}{\partial t} = -\mathscr{X}_1 - \frac{\beta_1^- + \beta_1^+}{2}\rho\frac{\partial u_2}{\partial x_2} \tag{A1}$$

$$\frac{\partial u_1}{\partial t} = -\mathscr{X}_3 + \frac{\beta_1^- - \beta_1^+}{2}c\frac{\partial u_2}{\partial x_2} \tag{A2}$$

$$\frac{\partial u_2}{\partial t} = -\mathscr{X}_4 - \frac{1}{\rho}\frac{\partial p}{\partial x_2} \tag{A3}$$

$$\frac{\partial p}{\partial t} = -\mathscr{X}_2 - \frac{\beta_1^- + \beta_1^+}{2}\rho c^2\frac{\partial u_2}{\partial x_2} \tag{A4}$$

where the convective and isotropic stress terms for the inviscid flows can be decomposed as

$$\mathscr{X}_1 \equiv \frac{1}{c^2}\left[\mathscr{I}_2 + \frac{1}{2}(\mathscr{I}_4 + \mathscr{I}_1)\right] \tag{A5}$$

$$\mathscr{X}_2 \equiv \tfrac{1}{2}(\mathscr{I}_4 + \mathscr{I}_1) \tag{A6}$$

$$\mathscr{X}_3 \equiv \frac{1}{2\rho c}(\mathscr{I}_4 - \mathscr{I}_1) \tag{A7}$$

$$\mathscr{X}_4 \equiv \mathscr{I}_3 \tag{A8}$$

and wave amplitude variations can be written in the following form:

$$\mathscr{I}_1 \equiv \rho c\boldsymbol{\lambda}_1 \cdot \nabla v_1 = (u_1 - c)\left(\frac{\partial p}{\partial x_1} - \rho c\frac{\partial u_1}{\partial x_1}\right) + u_2\left(\frac{\partial p}{\partial x_2} - \rho c\frac{\partial u_1}{\partial x_2}\right) \tag{A9}$$

$$\mathscr{I}_2 \equiv c^2\boldsymbol{\lambda}_2 \cdot \nabla v_2 = u_1\left(c^2\frac{\partial \rho}{\partial x_1} - \frac{\partial p}{\partial x_1}\right) + u_2\left(c^2\frac{\partial \rho}{\partial x_2} - \frac{\partial p}{\partial x_2}\right) \tag{A10}$$

DOI: 10.1002/fld

$$\mathscr{I}_3 \equiv -\boldsymbol{\lambda}_3 \cdot \nabla v_3 = u_1 \frac{\partial u_2}{\partial x_1} + u_2 \frac{\partial u_2}{\partial x_2} \tag{A11}$$

$$\mathscr{I}_4 \equiv \rho c \boldsymbol{\lambda}_4 \cdot \nabla v_4 = (u_1 + c)\left(\frac{\partial p}{\partial x_1} + \rho c \frac{\partial u_1}{\partial x_1}\right) + u_2 \left(\frac{\partial p}{\partial x_2} + \rho c \frac{\partial u_1}{\partial x_2}\right) \tag{A12}$$

The above equations for the primitive variables can be transformed to equations for conservative variables. Substitution of the above $\mathscr{X}_i$ expressions into the nondimensional equations result in the following set of equations at the x_1 boundaries for the conservative variables:

$$\frac{\partial \rho}{\partial t} = -\mathscr{X}_1 - \frac{\beta_1^- + \beta_1^+}{2} \rho \frac{\partial u_2}{\partial x_2} \tag{A13}$$

$$\frac{\partial m_1}{\partial t} = -u_1 \mathscr{X}_1 - \rho \mathscr{X}_3 - \frac{\beta_1^- + \beta_1^+}{2} \rho u_1 \frac{\partial u_2}{\partial x_2} + \frac{\beta_1^- - \beta_1^+}{2} \rho c \frac{\partial u_2}{\partial x_2} + \frac{1}{Re_a} \frac{\partial \tau_{1j}}{\partial x_j} \tag{A14}$$

$$\frac{\partial m_2}{\partial t} = -u_2 \mathscr{X}_1 - \rho \mathscr{X}_4 - \frac{\beta_1^- + \beta_1^+}{2} \rho u_2 \frac{\partial u_2}{\partial x_2} - \frac{\partial p}{\partial x_2} + \frac{1}{Re_a} \frac{\partial \tau_{2j}}{\partial x_j} \tag{A15}$$

$$\begin{aligned} \frac{\partial e}{\partial t} = & -\frac{1}{2} u_j^2 \mathscr{X}_1 - \frac{\mathscr{X}_2}{\gamma - 1} - \rho u_1 \mathscr{X}_3 - \rho u_2 \mathscr{X}_4 - u_2 \frac{\partial p}{\partial x_2} \\ & + \left[-\frac{\beta_1^- + \beta_1^+}{2} \left(\frac{\rho c^2 - p}{\gamma - 1} + e \right) + \frac{\beta_1^- - \beta_1^+}{2} \rho u_1 c \right] \frac{\partial u_2}{\partial x_2} \\ & + \frac{1}{Re_a} \frac{\partial}{\partial x_j} (u_i \tau_{ij}) + \frac{1}{Re_a Pr(\gamma - 1)} \frac{\partial}{\partial x_j} \left(\mu \frac{\partial T}{\partial x_j} \right) \end{aligned} \tag{A16}$$

For the left boundary, $\beta_1^- = 1$ and $\beta_1^+ = u_1/c$. For the right boundary, $\beta_1^+ = 1$ and $\beta_1^- = u_1/c$.

A.2. 2-D characteristic boundary conditions in x_2 direction

Similarly, for the x_2 boundaries, wave amplitude variations can be written in the following form:

$$\mathscr{J}_1 = (u_2 - c)\left(\frac{\partial p}{\partial x_2} - \rho c \frac{\partial u_2}{\partial x_2}\right) + u_1 \left(\frac{\partial p}{\partial x_1} - \rho c \frac{\partial u_2}{\partial x_1}\right) \tag{A17}$$

$$\mathscr{J}_2 = u_2 \left(c^2 \frac{\partial \rho}{\partial x_2} - \frac{\partial p}{\partial x_2}\right) + u_1 \left(c^2 \frac{\partial \rho}{\partial x_1} - \frac{\partial p}{\partial x_1}\right) \tag{A18}$$

$$\mathscr{J}_3 = u_2 \frac{\partial u_1}{\partial x_2} + u_1 \frac{\partial u_1}{\partial x_1} \tag{A19}$$

$$\mathscr{J}_4 = (u_2 + c)\left(\frac{\partial p}{\partial x_2} + \rho c \frac{\partial u_2}{\partial x_2}\right) + u_1 \left(\frac{\partial p}{\partial x_1} + \rho c \frac{\partial u_2}{\partial x_1}\right) \tag{A20}$$

DOI: 10.1002/fld

The convective and isotropic stress terms for the inviscid flows can be decomposed as

$$\mathscr{Y}_1 \equiv \frac{1}{c^2}\left[\mathscr{J}_2 + \frac{1}{2}(\mathscr{J}_4 + \mathscr{J}_1)\right] \tag{A21}$$

$$\mathscr{Y}_2 \equiv \tfrac{1}{2}(\mathscr{J}_4 + \mathscr{J}_1) \tag{A22}$$

$$\mathscr{Y}_3 \equiv \mathscr{J}_3 \tag{A23}$$

$$\mathscr{Y}_4 \equiv \frac{1}{2\rho c}(\mathscr{J}_4 - \mathscr{J}_1) \tag{A24}$$

The following set of equations at the x_2 boundaries for the conservative variables are solved:

$$\frac{\partial \rho}{\partial t} = -\mathscr{Y}_1 - \frac{\beta_2^- + \beta_2^+}{2}\rho\frac{\partial u_1}{\partial x_1} \tag{A25}$$

$$\frac{\partial m_1}{\partial t} = -u_1\mathscr{Y}_1 - \rho\mathscr{Y}_3 - \frac{\beta_2^- + \beta_2^+}{2}\rho u_1\frac{\partial u_1}{\partial x_1} - \frac{\partial p}{\partial x_1} + \frac{1}{Re_a}\frac{\partial \tau_{1j}}{\partial x_j} \tag{A26}$$

$$\frac{\partial m_2}{\partial t} = -u_2\mathscr{Y}_1 - \rho\mathscr{Y}_4 - \frac{\beta_2^- + \beta_2^+}{2}\rho u_2\frac{\partial u_1}{\partial x_1} + \frac{\beta_2^- - \beta_2^+}{2}\rho c\frac{\partial u_1}{\partial x_1} + \frac{1}{Re_a}\frac{\partial \tau_{2j}}{\partial x_j} \tag{A27}$$

$$\begin{aligned}\frac{\partial e}{\partial t} = &-\frac{1}{2}u_j^2\mathscr{Y}_1 - \frac{\mathscr{Y}_2}{\gamma-1} - \rho u_1\mathscr{Y}_3 - \rho u_2\mathscr{Y}_4 - u_1\frac{\partial p}{\partial x_1} \\ &+\left[-\frac{\beta_2^- + \beta_2^+}{2}\left(\frac{\rho c^2 - p}{\gamma-1} + e\right) + \frac{\beta_2^- - \beta_2^+}{2}\rho u_2 c\right]\frac{\partial u_1}{\partial x_1} \\ &+\frac{1}{Re_a}\frac{\partial}{\partial x_j}(u_i\tau_{ij}) + \frac{1}{Re_a Pr(\gamma-1)}\frac{\partial}{\partial x_j}\left(\mu\frac{\partial T}{\partial x_j}\right)\end{aligned} \tag{A28}$$

A.3. Extension to scalar transport properties

The multidimensional characteristic boundary conditions can be extended to the equations of the scalar transport properties in the nondimensional form,

$$\frac{\partial \rho Y_i}{\partial t} = -\frac{\partial}{\partial x_j}(\rho Y_i u_j) + S_i, \quad i = 1, 2, \ldots, m \tag{A29}$$

where S_i are source terms, and the corresponding Euler equations for the primitive variables become

$$\frac{\partial Y_i}{\partial t} = -\mathbf{u}\cdot\nabla Y_i \tag{A30}$$

DOI: 10.1002/fld

which is also of the characteristic form. Some examples are the vorticity equation, multiple species equations, and the turbulent kinetic energy equation in the URANS model:

$$\frac{\partial \omega}{\partial t} = -\mathbf{u}\cdot\nabla\omega + \frac{1}{Re_a}\frac{\partial}{\partial x_j}\left(\mu\frac{\partial \omega}{\partial x_j}\right) \tag{A31}$$

$$\frac{\partial \rho Y_i}{\partial t} = -\frac{\partial}{\partial x_j}(\rho Y_i u_j) + \frac{1}{Re_a Sc_i(\gamma-1)}\frac{\partial}{\partial x_j}\left(\mu\frac{\partial Y_i}{\partial x_j}\right) + \dot{\omega}_i \tag{A32}$$

$$\frac{\partial \rho k}{\partial t} = -\frac{\partial}{\partial x_j}(\rho k u_j) + \frac{1}{Re_a}\left(\tau_{ij} - \frac{2}{3}\rho k\delta_{ij}\right)\frac{\partial u_i}{\partial x_j} + \frac{1}{Re_a}\frac{\partial}{\partial x_j}\left[(\mu+\sigma^*\mu_T)\frac{\partial k}{\partial x_j}\right] - Re_a\rho\beta^* k\omega \tag{A33}$$

From the above characteristic forms, more characteristic variables and corresponding equations in the characteristic form can be written as

$$dv_{4+i} = dY_i, \quad \frac{\partial v_{4+i}}{\partial t} + \boldsymbol{\lambda}_{4+i}\cdot\nabla v_{4+i} = 0 \tag{A34}$$

where eigenvalues are $\boldsymbol{\lambda}_{4+i} = \mathbf{u}$. Similar to Hedstrom's method, the incoming waves and the outgoing waves can be identified and, correspondingly, the nonreflecting boundary conditions can be achieved by setting the magnitudes of the incoming waves to zero. For the x_1 boundaries, wave amplitude variations can be written in the following form:

$$\mathscr{I}_{4+i} \equiv \boldsymbol{\lambda}_{4+i}\cdot\nabla v_{4+i} = u_1\frac{\partial Y_i}{\partial x_1} + u_2\frac{\partial Y_i}{\partial x_2} \tag{A35}$$

Then, the convective and isotropic stress terms for the inviscid flows can be decomposed as

$$\mathscr{X}_{4+i} \equiv \mathscr{I}_{4+i} \tag{A36}$$

and the equations for the scalar-transport properties in conservative variables become

$$\frac{\partial \rho Y_i}{\partial t} = -Y_i\mathscr{X}_1 - \frac{(\beta_1^- + \beta_1^+)}{2}\rho Y_i\frac{\partial u_2}{\partial x_2} - \rho\mathscr{X}_{4+i} + S_i, \quad i = 1, 2, \ldots, m \tag{A37}$$

A.4. 3-D characteristic boundary conditions

For the x_1 boundaries wave amplitude variations can be written in the following form:

$$\mathscr{I}_1 = (u_1 - c)\left(\frac{\partial p}{\partial x_1} - \rho c\frac{\partial u_1}{\partial x_1}\right) + \sum_{j=2}^{3} u_j\left(\frac{\partial p}{\partial x_j} - \rho c\frac{\partial u_1}{\partial x_j}\right) \tag{A38}$$

$$\mathscr{I}_2 = u_j\left(c^2\frac{\partial \rho}{\partial x_j} - \frac{\partial p}{\partial x_j}\right) \tag{A39}$$

$$\mathscr{I}_3 = u_j\frac{\partial u_2}{\partial x_j} \tag{A40}$$

$$\mathscr{I}_4 = u_j\frac{\partial u_3}{\partial x_j} \tag{A41}$$

DOI: 10.1002/fld

$$\mathscr{I}_5=(u_1+c)\left(\frac{\partial p}{\partial x_1}+\rho c\frac{\partial u_1}{\partial x_1}\right)+\sum_{j=2}^{3}u_j\left(\frac{\partial p}{\partial x_j}+\rho c\frac{\partial u_1}{\partial x_j}\right) \tag{A42}$$

$$\mathscr{I}_{5+i}=u_j\frac{\partial Y_i}{\partial x_j} \tag{A43}$$

Then the convective and isotropic stress terms for the inviscid flows can be decomposed as

$$\mathscr{X}_1\equiv\frac{1}{c^2}\left[\mathscr{I}_2+\frac{1}{2}(\mathscr{I}_4+\mathscr{I}_1)\right],\quad \mathscr{X}_2\equiv\frac{1}{2}(\mathscr{I}_4+\mathscr{I}_1) \tag{A44}$$

$$\mathscr{X}_3\equiv\frac{1}{2\rho c}(\mathscr{I}_4-\mathscr{I}_1),\quad \mathscr{X}_4\equiv\mathscr{I}_3,\quad \mathscr{X}_5\equiv\mathscr{I}_4,\quad \mathscr{X}_{5+i}\equiv\mathscr{I}_{5+i} \tag{A45}$$

and the nonreflecting boundary conditions are achieved by solving the equations for the conservative variables:

$$\frac{\partial\rho}{\partial t}=-\mathscr{X}_1-\frac{\beta_1^-+\beta_1^+}{2}\rho\sum_{j=2}^{3}\frac{\partial u_j}{\partial x_j} \tag{A46}$$

$$\frac{\partial m_1}{\partial t}=-u_1\mathscr{X}_1-\rho\mathscr{X}_3-\frac{\beta_1^-+\beta_1^+}{2}\rho u_1\sum_{j=2}^{3}\frac{\partial u_j}{\partial x_j}+\frac{\beta_1^--\beta_1^+}{2}\rho c\sum_{j=2}^{3}\frac{\partial u_j}{\partial x_j}+\frac{1}{Re_a}\frac{\partial\tau_{1j}}{\partial x_j} \tag{A47}$$

$$\frac{\partial m_2}{\partial t}=-u_2\mathscr{X}_1-\rho\mathscr{X}_4-\frac{\beta_1^-+\beta_1^+}{2}\rho u_2\sum_{j=2}^{3}\frac{\partial u_j}{\partial x_j}-\frac{\partial p}{\partial x_2}+\frac{1}{Re_a}\frac{\partial\tau_{2j}}{\partial x_j} \tag{A48}$$

$$\frac{\partial m_3}{\partial t}=-u_3\mathscr{X}_1-\rho\mathscr{X}_5-\frac{\beta_1^-+\beta_1^+}{2}\rho u_3\sum_{j=2}^{3}\frac{\partial u_j}{\partial x_j}-\frac{\partial p}{\partial x_3}+\frac{1}{Re_a}\frac{\partial\tau_{3j}}{\partial x_j} \tag{A49}$$

$$\begin{aligned}\frac{\partial e}{\partial t}=&-\frac{1}{2}u_j^2\mathscr{X}_1-\frac{\mathscr{X}_2}{\gamma-1}-\rho u_1\mathscr{X}_3-\rho u_2\mathscr{X}_4-\rho u_3\mathscr{X}_5-\sum_{j=2}^{3}u_j\frac{\partial p}{\partial x_j}\\&+\left[-\frac{\beta_1^-+\beta_1^+}{2}\left(\frac{\rho c^2-p}{\gamma-1}+e\right)+\frac{\beta_1^--\beta_1^+}{2}\rho u_1 c\right]\sum_{j=2}^{3}\frac{\partial u_j}{\partial x_j}\\&+\frac{1}{Re_a}\frac{\partial}{\partial x_j}(u_i\tau_{ij})+\frac{1}{Re_aPr(\gamma-1)}\frac{\partial}{\partial x_j}\left(\mu\frac{\partial T}{\partial x_j}\right)\end{aligned} \tag{A50}$$

$$\frac{\partial\rho Y_i}{\partial t}=-Y_i\mathscr{X}_1-\rho\mathscr{X}_{5+i}+S_i,\quad i=1,2,\ldots,m \tag{A51}$$

For the left boundary, $\beta_1^-=1$ and $\beta_1^+=u_1/c$. For the right boundary, $\beta_1^+=1$ and $\beta_1^-=u_1/c$.

ACKNOWLEDGEMENTS

Partial support for this work was provided by the National Aeronautics and Space Administration (NASA) under grant No. NAG-1-02116 and the National Science Foundation (NSF) under grants No. EAR-0242591, EAR-0327269 and ACI-0242457. This support is gratefully acknowledged.

DOI: 10.1002/fld

REFERENCES

1. Givoli D. Non-reflecting boundary conditions. *Journal of Computational Physics* 1991; **94**:1–29.
2. Tsynkov SV. Numerical solution of problems on unbounded domains—a review. *Applied Numerical Mathematics* 1998; **27**:465–532.
3. Hagstrom T. Radiation boundary conditions for the numerical simulation of waves. *Acta Numerica* 1999; **8**:47–106.
4. Colonius T. Modeling artificial boundary conditions for compressible flow. *Annual Review of Fluid Mechanics* 2004; **36**:315–345.
5. Engquist B, Majda A. Absorbing boundary conditions for the numerical simulation of waves. *Mathematics of Computation* 1977; **31**:629–651.
6. Engquist B, Majda A. Radiation boundary conditions for acoustic and elastic wave calculations. *Communications on Pure and Applied Mathematics* 1979; **32**:313–357.
7. Bayliss A, Turkel E. Radiation boundary conditions for wave-like equations. *Communications on Pure and Applied Mathematics* 1980; **33**:707–725.
8. Bayliss A, Turkel E. Far field boundary conditions for compressible flows. *Journal of Computational Physics* 1982; **48**:182–199.
9. Hu FQ. On absorbing boundary conditions for linearized Euler equations by a perfectly matched layer. *Journal of Computational Physics* 1996; **129**:201–219.
10. Hu FQ. A stable, perfectly matched layer fpr linearized Euler equations in unsplit physical variables. *Journal of Computational Physics* 2001; **173**:455–480.
11. Freund JB. Proposed inflow/outflow boundary condition for direct computation of aerodynamic sound. *AIAA Journal* 1997; **35**:740–742.
12. Nordstrom J, Carpenter MH. Boundary and interface conditions for high-order finite-difference methods applied to the Euler and Navier–Stokes equations. *Journal of Computational Physics* 1999; **148**:621–645.
13. Poinsot T, Lele S. Boundary conditions for direct simulations of compressible viscous flows. *Journal of Computational Physics* 1992; **101**:104–129.
14. Hedstrom GW. Nonreflecting boundary conditions for nonlinear hyperbolic systems. *Journal of Computational Physics* 1979; **30**:222–237.
15. Thompson KW. Time-dependent boundary conditions for hyperbolic systems. *Journal of Computational Physics* 1987; **68**:1–24.
16. Thompson KW. Time-dependent boundary conditions for hyperbolic systems, ii. *Journal of Computational Physics* 1990; **89**:439–461.
17. Baum M, Poinsot TJ, Thevenin D. Accurate boundary conditions for multicomponent reactive flows. *Journal of Computational Physics* 1994; **116**:247–261.
18. Moureau V, Lartigue G, Sommerer Y, Angelberger C, Colin O, Poinsot T. Numerical methods for unsteady compressible multi-component reacting flows on fixed and moving grids. *Journal of Computational Physics* 2005; **202**:710–736.
19. Okong'o N, Bellan J. Consistent boundary conditions for multicomponent real gas mixtures based on characteristic waves. *Journal of Computational Physics* 2002; **176**:330–344.
20. Kim JW, Lee DJ. Generalized characteristric boundary conditions for computational aeroacoustics. *AIAA Journal* 2000; **38**:2040–2049.
21. Kim JW, Lee DJ. Generalized characteristric boundary conditions for computational aeroacoustics, part 2. *AIAA Journal* 2004; **42**:47–55.
22. Nicoud F. Defining wave amplitude in characteristic boundary conditions. *Journal of Computational Physics* 1999; **149**:418–422.
23. Sutherland JC, Kennedy CA. Improved boundary conditions for viscous, reacting, compressible flows. *Journal of Computational Physics* 2003; **191**:502–524.
24. Prosser R. Improved boundary conditions for the direct numerical simulation of turbulent subsonic flows. I. Inviscid flows. *Journal of Computational Physics* 2005; **207**:736–768.
25. Prosser R. Toward improved boundary conditions for the dns and les of turbulent subsonic flows. *Journal of Computational Physics* 2007; **222**:469–474.
26. Yoo CS, Wang Y, Trouve A, Im HG. Characteristic boundary conditions for direct simulations of turbulent counterflow flames. *Combustion Theory and Modelling* 2005; **9**:617–646.
27. Yoo CS, Im HG. Characteristic boundary conditions for simulations of compressible reacting flows with multidimensional, viscous and reaction effects. *Combustion Theory and Modelling* 2007; **11**:259–286.

DOI: 10.1002/fld

28. Rudy DH, Strikwerda JC. A non-reflecting outflow boundary condition for subsonic Navier–Stokes calculations. *Journal of Computational Physics* 1980; **36**:55–70.
29. Liu Q. An integrated modeling and simulation approach for flow-generated sound prediction. *Ph.D. Dissertation*, Department of Mechanical Engineering, University of Colorado, Boulder, CO, 2007.
30. Laney CB. *Computational Gasdynamics*. Cambridge University Press: Cambridge, 1998.
31. Deconinck H. Analysis of wave propagation properties for the euler equations in two space dimensions. In *Computational Fluid Dynamics*, Deconinck H (ed.). Lecture Series—Von Karman Institute for Fluid Dynamics, vol. 5. Von Karman Institute: Brussels, Belgium, 1994; J1–J25.
32. Deconinck H, Hirsch C, Peuteman J. Characteristic decomposition methods for the multidimensional Euler equations. In *10th International Conference on Numerical Methods in Fluid Dynamics*, Araki H *et al.* (eds). Lecture Notes in Physics, vol. 264. Springer: Beijing, 1986; 216–221.
33. Hirsch C. A diagonalization procedure for the multidimensional Euler equations. In *Proceedings of High Speed Aerodynamics I*, Nastase A (ed.). Haag+Herchen: T.H. Aachen, 1986; 69–75.
34. Anderson JD. *Fundamentals of Aerodynamics*. McGraw-Hill: New York, 2001.
35. Tam CKW, Hardin JC (eds). Second Computational Aeroacoustics (CAA) Workshop on Benchmark Problems. *NASA Conference Publication 3352*, 1997.
36. Tam CKW. Derivation of an exact solution for the scattering of an acoustic pulse by a circular cylinder. *Private Communication*, 2005.
37. Colonius T, Lele SK, Moin P. Boundary conditions for direct computation of aerodynamic sound generation. *AIAA Journal* 1993; **31**:1574–1582.
38. Rowley CW, Colonius T. Discretely nonreflecting boundary conditions for linear hyperbolic systems. *Journal of Computational Physics* 2000; **157**:500–538.
39. Liu Q, Vasilyev OV. Hybrid adaptive wavelet collocation–brinkman penalization method for unsteady rans simulations of compressible flow around bluff bodies. *AIAA Paper No. 2006-3206*, 2006.
40. Liu Q, Vasilyev OV. A brinkman penalization method for compressible flows in complex geometries. *Journal of Computational Physics* 2007; **227**:946–966.

DOI: 10.1002/fld